J. Fluid Mech. (2009), *vol.* 629, *pp.* 263–298.
doi:10.1017/S002211200900634X Printed in the United Kingdom

On the origin of the inflectional instability of a laminar separation bubble

SOURABH S. DIWAN AND O. N. RAMESH†

Department of Aerospace Engineering, Indian Institute of Science, Bangalore 560012, India

(Received 30 October 2007 and in revised form 22 January 2009)

This is an experimental and theoretical study of a laminar separation bubble and the associated linear stability mechanisms. Experiments were performed over a flat plate kept in a wind tunnel, with an imposed pressure gradient typical of an aerofoil that would involve a laminar separation bubble. The separation bubble was characterized by measurement of surface-pressure distribution and streamwise velocity using hot-wire anemometry. Single component hot-wire anemometry was also used for a detailed study of the transition dynamics. It was found that the so-called dead-air region in the front portion of the bubble corresponded to a region of small disturbance amplitudes, with the amplitude reaching a maximum value close to the reattachment point. An exponential growth rate of the disturbance was seen in the region upstream of the mean maximum height of the bubble, and this was indicative of a linear instability mechanism at work. An infinitesimal disturbance was impulsively introduced into the boundary layer upstream of separation location, and the wave packet was tracked (in an ensemble-averaged sense) while it was getting advected downstream. The disturbance was found to be convective in nature. Linear stability analyses (both the Orr–Sommerfeld and Rayleigh calculations) were performed for mean velocity profiles, starting from an attached adverse-pressure-gradient boundary layer all the way up to the front portion of the separation-bubble region (i.e. up to the end of the dead-air region in which linear evolution of the disturbance could be expected). The conclusion from the present work is that the primary instability mechanism in a separation bubble is inflectional in nature, and its origin can be traced back to upstream of the separation location. In other words, the inviscid inflectional instability of the separated shear layer should be logically seen as an extension of the instability of the upstream attached adverse-pressure-gradient boundary layer. This modifies the traditional view that pegs the origin of the instability in a separation bubble to the detached shear layer outside the bubble, with its associated Kelvin–Helmholtz mechanism. We contend that only when the separated shear layer has moved considerably away from the wall (and this happens near the maximum-height location of the mean bubble), a description by the Kelvin–Helmholtz instability paradigm, with its associated scaling principles, could become relevant. We also propose a new scaling for the most amplified frequency for a wall-bounded shear layer in terms of the inflection-point height and the vorticity thickness and show it to be universal.

1. Introduction

The separation of a laminar boundary layer from a solid surface is prevalent in very many flow situations such as over gas turbine blades (especially in the low-pressure

† Email address for correspondence: onr@aero.iisc.ernet.in

turbine stage) and the wings of micro aero vehicles (MAVs) that operate at fairly low Reynolds numbers. Flow separation occurs in such cases due to the presence of an adverse pressure gradient. These are instances of the so-called pressure-gradient-induced separation, to be contrasted with 'geometry-induced' separation as that over a sharp corner. The separated shear layer becomes unstable due to the presence of an inflection point and presumably transitions to turbulence rapidly. Eventually, there is reattachment back to the solid surface further downstream, if conditions are conducive. The region enclosed by the shear layer is called a separation bubble and has been a subject of many studies in the past.

One of the earliest surveys of the literature was that of Tani (1964). Most of the work reported therein was done on the suction surface of a variety of aerofoil configurations at different angles of attack. It was observed that at relatively small angles of attack, the length of the separation bubble reduced with an increase in angle of attack till a critical condition was reached when there was a sudden increase in the length of the bubble. This phenomenon was termed 'bursting' of the bubble, and most of the early work was done towards devising empirical criteria to predict bursting, since it was seen to be directly related to the stalling of the aerofoil.

A two-parameter bursting criterion was suggested by Gaster (1967) that is by far the most cited one. Apart from attempting to rationally characterize the bursting phenomenon, Gaster's work (Gaster 1967) is remarkable for going beyond merely suggesting an empirical criterion and having explored the physics of the transition process in the separation bubble.

In many of the relatively recent studies, the focus has been directed towards the dominant transition mechanism in the unstable separated shear layer. Pauley, Moin & Reynolds (1990), by two-dimensional numerical simulation studies, found the laminar separation bubble to become unsteady with a corresponding shedding of vortices from the bubble for relatively large values of adverse pressure gradient. This was attributed to the inviscid instability of the detached shear layer.

Watmuff (1999) carried out a detailed experimental study of a two-dimensional laminar separation bubble. Watmuff (1999) introduced wave packets into the boundary layer by means of periodic forcing to study the stability characteristics. Based on the results obtained using stationary hot-wire anemometry (and a limited amount of flying hot-wire anemometry studies), he concluded that the primary instability must be an inviscid inflectional mechanism typical of Kelvin–Helmholtz instability for the following reasons: (*a*) the appearance of a cat's-eye pattern in the vorticity contour; (*b*) occurrence of maximum disturbance amplitude at the inflection point; (*c*) good match obtained between the dominant frequency in the experiment and the most amplified frequency obtained from the analysis of Monkewitz & Huerre (1982) for a free shear layer, near the maximum-height location.

Dovgal, Kozlov & Michalke (1994) presented a comprehensive review of the stability characteristics of a separation bubble. They performed linear stability calculations for an analytical velocity profile typical of that found in a separation bubble, consisting of forward velocity in the outer region along with a small reversed flow in the neighbourhood of the wall. Both the pressure-gradient-induced and geometry-induced bubbles were considered. They showed that the instability of the separated shear layer was similar to the instability of the free shear layer and commented that the viscous mechanism assumed importance only when the separation bubble was very small.

Based on their direct numerical simulation (DNS) study of a 'short' separation bubble, Alam & Sandham (2000) concluded that the separated shear layer undergoes transition via oblique modes and lambda-vortex-induced breakdown. Haggmark,

Bakchinov & Alfredsson (2000), from their experimental investigation, attributed a dominant role to the inviscid instability mechanism in the separated shear layer. Marxen *et al.* (2003) performed a linear stability analysis of the base profiles (obtained from a DNS study) and found the viscous Tollmien–Schlichting (TS) instability to be the primary instability mechanism. Spalart & Strelets (2000), in their DNS study, eliminated the incoming disturbances in the entry region of the boundary layer. They found that transition took place by some sort of bypass mechanism that they called 'transition by contact'.

To summarize, significant progress has been made so far on various aspects of the linear stability of a separation bubble, and most of the studies point to the inviscid instability associated with the separated shear layer to be the main mechanism. The present work is an effort to understand the exact origin of the primary instability mechanism responsible for the amplification of disturbances. We argue that at least up to the front portion of the bubble (up to a location slightly upstream of the maximum mean height of the bubble over which linear evolution of disturbances is observed), the instability mechanism is due to the inflectional mode associated with the mean velocity profile. However, the seeds of this inviscid inflectional instability could be traced back to the adverse-pressure-gradient boundary layer upstream of separation. The upstream boundary layer is convectively unstable, and hence the disturbance from there gets advected downstream to the separation-bubble region. And it is only when the shear layer has moved sufficiently far away from the wall after separation that the disturbance dynamics become nearly indistinguishable from the free shear layer instability of the classical type that is describable by the Kelvin–Helmholtz instability paradigm. While this conclusion of the present study is in agreement with the previous studies as far as the role of the inviscid inflectional instability is concerned, the new element here is the identification of the attached-boundary-layer region upstream of separation as the origin of this instability. In the course of arriving at this conclusion, we have introduced a new scaling principle for the most amplified frequency of the disturbance in terms of the distance of the inflection point from the wall and the vorticity thickness (as defined by Monkewitz & Huerre 1982).

Section 2 describes the details of the experimental set-up and measurement techniques. In § 3, we present the results of the separation bubble without any excitation. Section 4 concerns the response of a separation bubble to external excitation and the evolution of the resulting wave packets through the bubble. The questions of the origin of the inflectional instability of the bubble and the scaling of the most amplified frequency are considered in § 5. A discussion of the importance of the present findings is given in § 6. Finally, conclusions are presented in § 7.

2. Experimental set-up and measurement techniques

Experiments have been conducted in a closed-circuit wind tunnel at the Department of Aerospace Engineering, Indian Institute of Science. The test section is 1 m × 1 m in cross-section and 4 m long. The turbulence intensity in the test section of the tunnel, defined as the root mean square (r.m.s.) of the streamwise fluctuating velocity divided by the mean streamwise velocity and multiplied by hundred (i.e. $Tu = (\sqrt{\overline{u'^2}}/U) \times 100$), is relatively low ($\approx$0.03 %) as measured on the centreline. This makes it suitable for transition studies in which a quiet disturbance environment is highly desirable. The experimental set-up is shown in figure 1.

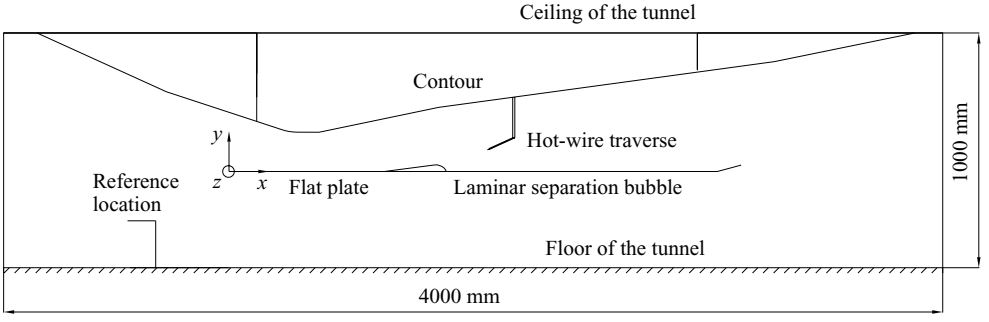

FIGURE 1. Experimental set-up.

A 5 mm thick aluminium plate that was 1 m wide and 2 m long was mounted in the test section on six supports fastened to the sidewalls of the tunnel. The plate rested on a skeleton of steel angle ribs and struts, so as to avoid bending. Levelling screws were provided with the help of which the plate could be set at any angle of incidence relative to the flow. The plate had a super-elliptic leading edge to promote attached laminar flow over the forward part of the plate (Narasimha & Prasad 1994). A small flap was hinged at the rear of the plate. It was deflected so as to move the front stagnation point forward on the upper surface of the plate to account for any possible asymmetry of the oncoming flow. In order to measure surface-pressure distribution, holes of 0.7 mm diameter were drilled on the plate at 39 streamwise stations.

The adverse pressure gradient was applied on the flat plate by contouring the top wall of the tunnel. The contour was a wooden skeleton covered up by a polycarbonate sheet. The contour could be moved down as a whole or tilted by using a screw-rod arrangement at two streamwise locations. By different combinations of the pivots, the contour at the ceiling could be set to various streamwise distributions of adverse pressure gradient. The ceiling setting used in the present experiments is shown in figure 1. A brass trip wire was stuck to the ceiling, and it was made sure that the boundary layer did not separate there by tuft flow-visualization and surface flow-visualization techniques during preliminary exploratory studies. A slot was made on the ceiling along the centreline so as to enable the traverse arm, with hot-wire probe attached to its end, to be introduced into the flow.

Sunshine Industries model no. 717 constant-temperature hot-wire anemometer (CTA) was used for making streamwise velocity measurements in the flow. The hot-wire probe was made up of 5 μm diameter tungsten wire. The wire was spot-welded to the prongs of the holder. The length to diameter ratio of the wire was kept between 300 and 400. The probe was calibrated before and after each experiment, and if there was a large drift in calibration, the whole data was discarded.

A Cartesian coordinate system is shown in figure 1 with x, y and z representing streamwise, wall-normal and spanwise directions respectively. The corresponding mean velocity components are U, V and W. All the measurements in the present work have been done along the centreline of the plate with a stationary hot-wire anemometry measuring streamwise velocity (U) only. The origin of the coordinate system is located at the leading edge of the plate on the centreline. The data was acquired at the rate of 2 KHz using the virtual instrumentation software DASYLab.

Artificial disturbance was introduced into the flow through one of the pressure ports using a loudspeaker. The loudspeaker was driven by an electronic driver that supplied square waves of narrow width (having duration of 10 ms), at regular intervals of 1 s. This forcing serves as a close approximation to the periodic impulsive forcing.

Hatman & Wang (1998), Watmuff (1999) and Haggmark *et al.* (2000) have discussed the difficulties associated with the stationary hot-wire anemometry as a measurement tool for separation bubbles. The issues involved can be summarized as follows:

(i) The stationary hot wire is insensitive to the direction of the flow. This puts serious restrictions on using it for exploring the structure of the separation bubble in which reversed flow is present. Furthermore, the flow field in the rear portion of the bubble is highly unsteady. As a result, rectification of hot-wire signals will occur if there is a change in sign of the velocity due to large unsteadiness. From Watmuff (1999), the errors involved in the reversed-flow measurements are estimated to be around 10 %–20 % of the free-stream velocity.

(ii) The presence of the hot wire itself might alter the shape and size of the separation bubble. In the present study, it was observed that placing the hot wire in the separated shear layer above (and outside) the mean dividing streamline of the bubble did not have significant effect on the bubble. But when the hot wire was introduced inside the bubble, there was modification of its shape and size. These features were observed during the preliminary smoke flow-visualization studies. It was, however, not attempted to quantify the effect of the presence of hot wire on the bubble.

In this work, the time series data measured at the locus of maximum turbulence intensity (corresponding approximately to the locus of inflection points up to the maximum-height location) has been used for studying the disturbance dynamics. Since this location is well above the wall and outside the mean dividing streamline, the difficulty associated with reversed-flow measurement is not expected to be a problem. The time series data from the wall region, which was seen to be beset with measurement uncertainties, has not been used.

3. The unexcited separation bubble

The experiments have been done with two values of reference velocity – $U_{ref} = 2.78\,\mathrm{m\,s^{-1}}$ and $5.4\,\mathrm{m\,s^{-1}}$. The reference velocity was measured 430 mm upstream of the plate leading edge. In what follows, we will be reporting the results for the $U_{ref} = 2.78\,\mathrm{m\,s^{-1}}$ case primarily (corresponding to a separation bubble longer than that for the higher-speed case) for clarity of presentation. For discussion related to transition dynamics of the most amplified waves, to be discussed in § 5, experiments pertaining to the higher reference speed also will be presented to demonstrate the universality of the new scaling relation to be introduced therein. Hence, unless otherwise mentioned, all the experimental results correspond to $U_{ref} = 2.78\,\mathrm{m\,s^{-1}}$.

The pressure distribution along the centreline of the plate is shown in figure 2. The coefficient of pressure is given by

$$C_p = \frac{(P_x - P_{ref})}{(P_{total} - P_{ref})}, \tag{3.1}$$

where P_x is the pressure at a desired streamwise location; P_{total} is the total pressure measured by a reference Pitot-static tube located upstream of the flat plate (see figure 1); and P_{ref} is the static pressure at the reference location.

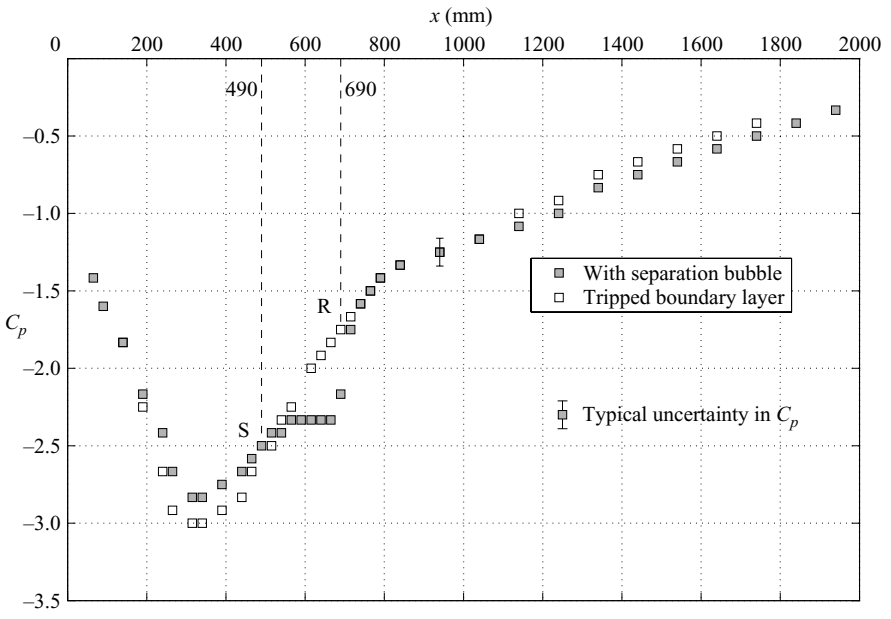

FIGURE 2. Coefficient of pressure distribution for $U_{ref} = 2.78\,\mathrm{m\,s^{-1}}$ with and without tripping the boundary layer.

The separation and reattachment locations are indicated in the pressure distribution plot by symbols S and R. The streamwise locations corresponding to separation, maximum height and reattachment for the mean bubble were determined to be 490 mm, 615 mm and 690 mm respectively. These locations have been inferred primarily from the hot-wire measurements and smoke flow-visualization studies. Furthermore, the hot-wire anemometry measurements and smoke flow-visualizations have been calibrated to infer separation and reattachment locations against the surface flow-visualization technique of Langston & Boyle (1982) that works well at relatively high speeds. The result of this calibration exercise is the conclusion that the hot-wire measurements can be conveniently used to identify mean separation and reattachment locations.

The pressure in the initial portion of the separation bubble is relatively constant as can be seen in figure 2. This 'dead-air' region is followed by a sharp pressure recovery further downstream. The boundary layer upstream of separation was tripped in order to achieve an inviscid pressure distribution on the plate, and this is also shown figure 2. It can be seen that the constant-pressure region disappears when the trip is introduced, thereby confirming that the phenomenon seen in the non-tripped case is indeed a laminar separation bubble.

The surface flow-visualization pattern (obtained by using 'ink-dot-matrix' technique, to be elaborated upon in Appendix A) showed that even though the basic tunnel flow (in the absence of bubble) and the attached boundary layer well upstream of separation are nominally two-dimensional, the resulting separation pattern is three-dimensional. Furthermore, this effect is felt even upstream of separation in that there is a certain degree of three-dimensionality observed for some distance upstream of the separation line. While this may appear surprising at first sight, this aspect of three-dimensionality in a nominally two-dimensional oncoming flow indeed turns out to be a topological necessity for the surface-streamline patterns involving a separation line.

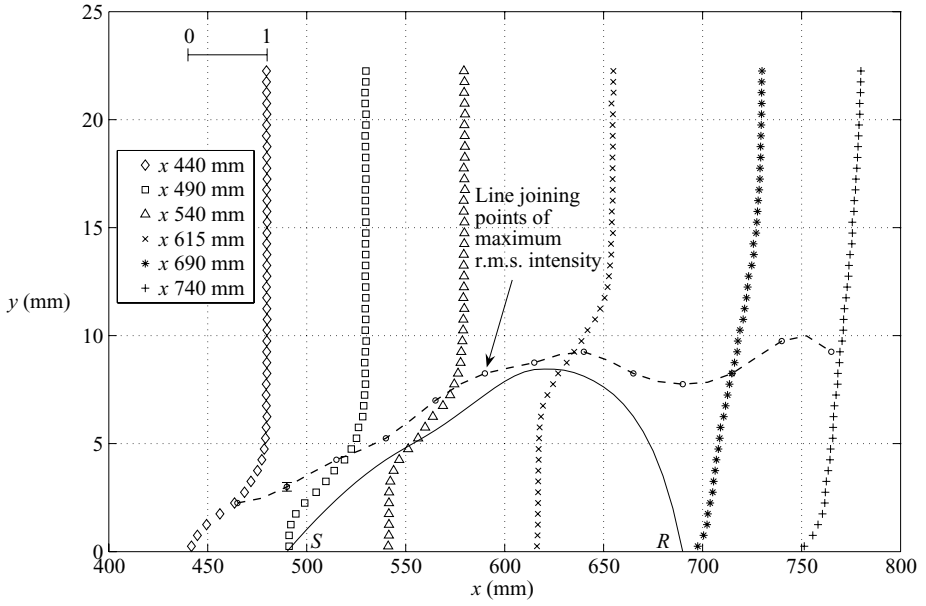

FIGURE 3. Normalized mean velocity profiles at different streamwise locations for $U_{ref} = 2.78\,\mathrm{m\,s^{-1}}$. The solid line represents the approximate bubble outline. An error bar is shown on the line of maximum r.m.s. intensity.

Following the suggestion of one of the referees, we have addressed this issue in detail in Appendix A in which the surface flow-visualization patterns are provided along with the surface-pressure distributions at three spanwise locations. A justification is also given therein for the use of centreline hot-wire measurements which have been performed in the present work.

Figure 3 shows the normalized mean velocity profiles at different streamwise locations for $U_{ref} = 2.78\,\mathrm{m\,s^{-1}}$. The approximate time-averaged bubble outline inferred from the analytical fits for the measured mean velocity profiles, to be introduced in § 5, is also indicated on the same plot with a continuous line; the height of the time-averaged separation bubble was found to be approximately 8.4 mm. The dashed line shown indicates the locus of maximum streamwise turbulence intensity locations at different streamwise stations. For the region up to the maximum-height location of the bubble, the dotted line matches approximately with the locus of inflection points of the mean velocity profile also. This is quite expected, since the large shear present at the point of inflection would greatly enhance the transfer of energy from the mean flow to the fluctuations. The reattached velocity profile does not correspond to the fully developed turbulent profile, and the relaxation towards equilibrium is slow. This observation is consistent with the findings of Alam & Sandham (2000). The velocity profile at the reattachment point (which is approximately linear in most of its part) is similar to the universal reattachment profile of Horton (1969).

The contour plot of r.m.s. fluctuation velocity normalized by the local free-stream velocity along with the mean bubble outline is shown in figure 4. Since the stationary hot-wire data inside the separation-bubble region is likely to be fraught with uncertainties, the region is excluded in figure 4 by showing it in white. The dashed

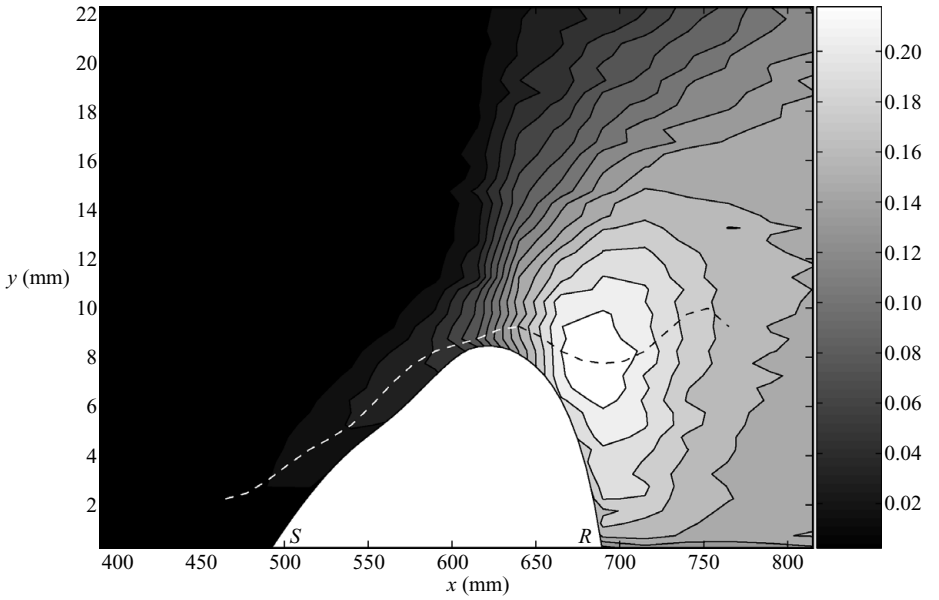

FIGURE 4. Contour plot of r.m.s. fluctuation velocity normalized by local free-stream velocity for $U_{ref} = 2.78\,\mathrm{m\,s^{-1}}$. The solid line is the approximate outline of the bubble, and the dashed line is the locus of maximum r.m.s. turbulence intensity locations at various streamwise stations.

line again is the line joining the locus of maximum turbulence intensity locations. The global maximum of turbulence intensity is observed at the reattachment point.

For attached flows, the location corresponding to one of the two maxima of turbulence intensity in the boundary layer is used to monitor the transition process; Gaster & Grant (1975) used the second maximum outside the transitional-boundary-layer mean edge. For separated flows, the inflection point at which the intensity has a peak value is used as the monitoring location (Watmuff 1999). Taking cue from these studies, we have chosen the locus of maximum turbulence intensity locations (dashed lines in figures 3 and 4) for monitoring the transition process and the evolution of disturbances in this study.

Figure 5 depicts the variation of maximum r.m.s. fluctuating velocity (normalized by local free-stream velocity, U_{fs}) with the streamwise distance. It shows moderate amplitudes of the disturbances upstream of the location of maximum height, whereas relatively large amplitudes are seen in the rear portion of the bubble. The amplitude reaches a maximum value at the reattachment location and then decays further downstream. This behaviour is consistent with the results of Watmuff (1999). It is interesting to compare the disturbance amplitude variation of the unexcited bubble with the corresponding static-pressure distribution, and this is also shown in figure 5. This shows that in the dead-air region, the amplitude of the disturbance is relatively low. It will be shown later (viz. figure 7) that the growth of disturbances in the initial portion of the bubble is exponential which is typical of a linear instability mechanism.

Studies on attached flow transition (Herbert 1988) find that nonlinearity sets in when the disturbance amplitude reaches a magnitude of about 1 % of the free-stream velocity. Betchov & Szewczyk (1963) also find from their theory that the threshold value for the onset of nonlinearity in free shear layers is 1 %. However, in the present case the exponential growth of the disturbance is observed even when the disturbance

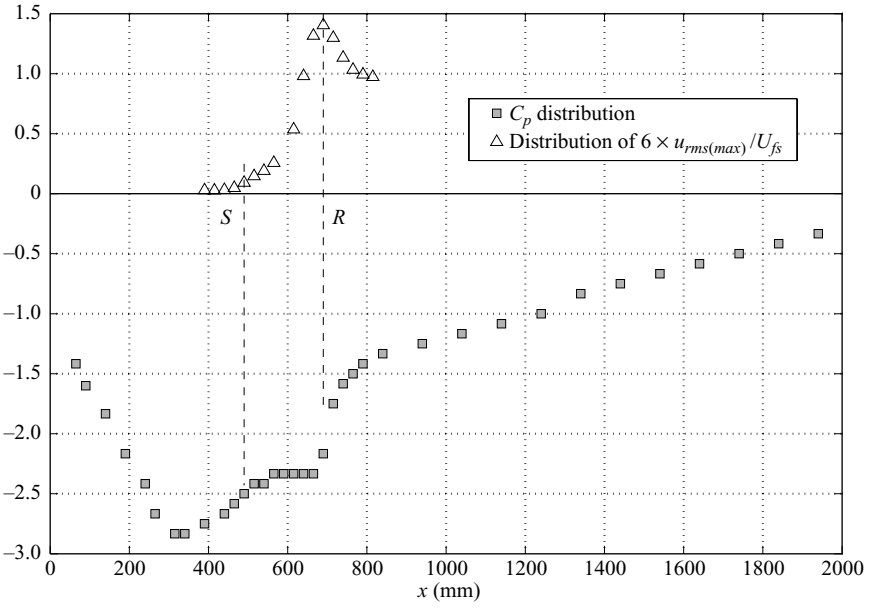

FIGURE 5. Distribution of maximum r.m.s. intensity in the streamwise direction along with the C_p plot for the separation bubble; $U_{ref} = 2.78\,\mathrm{m\,s^{-1}}$. (The y axis for r.m.s. intensity is magnified six times for clarity).

amplitude is nearly 10 % to 20 % of the free-stream velocity. This may be due to the fact that the threshold required to be crossed for the inception of nonlinear evolution is larger for separated flows than attached and free shear flows. Hence linear stability theories can still be employed till the nonlinearity threshold is reached for a separated flow. This observation finds support from the studies of Watmuff (1999) and Marxen *et al.* (2003) who find the persistence of linear behaviour up to the streamwise location at which the disturbance amplitude reaches 20 % and 10 % of the free-stream velocity respectively.

4. External excitation of the separation bubble

In order to study the stability characteristics of the separation bubble further, an artificial disturbance was introduced impulsively into the boundary layer that resulted in the generation of a wave packet a little distance downstream. The disturbance was introduced into the boundary layer through one of the pressure ports on the centreline. The location of introduction of the disturbance was chosen to be the peak-suction location at which C_p reaches a minimum value (upstream of separation; $x = 340\,\mathrm{mm}$). The initial amplitude of the disturbance was very small, and a smooth wavy structure was seen to persist for sufficiently large streamwise distance. The introduced wave packet thus behaved as an infinitesimal perturbation that was initially of the same order as natural perturbation.

All the fluctuating-velocity time traces were measured along the line joining locations of local maxima of r.m.s. intensity (as shown in figures 3 and 4) and were non-dimensionalized by the local free-stream velocity. The frequency of excitation was decided by trial and error and was fixed to be 1 Hz. It was ensured that the

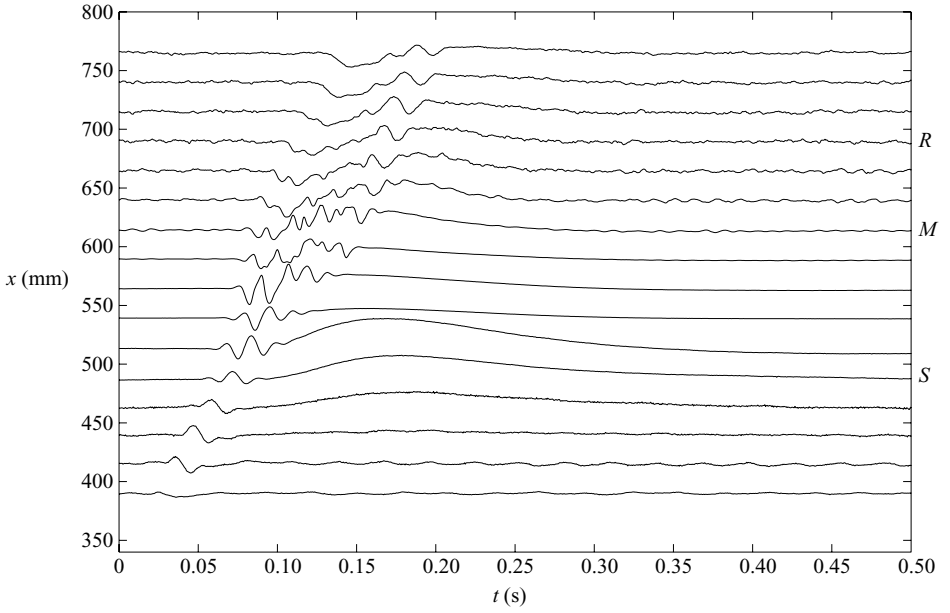

FIGURE 6. Evolution of the wave packet in the downstream direction. The disturbance is introduced at $x = 340$ mm; S, M and R indicate separation, maximum-height and reattachment locations for the unexcited case respectively; $U_{ref} = 2.78\,\mathrm{m\,s^{-1}}$.

separation bubble returned to the undisturbed position before the arrival of the next wave packet.

The fluctuating velocity at each position was acquired at a sampling rate of 2 KHz, and the duration of the time series was chosen so that it contained 128 realizations (or wave packets) in the ensemble. (Some limited exploratory studies were done with 256 realizations in the ensemble, but it did not change the basic ensemble-averaged results.) It was then phase-averaged with respect to the leading edge of the voltage pulse supplied to the speaker, and a distinct wave packet was observed at all streamwise locations. Ensemble-averaging eliminates the random noise to a great extent, since it is uncorrelated with the signal; for a Gaussian noise it is well known that the signal-to-noise ratio is proportional to a factor $\sqrt{N}$, where N is the number of realizations in the ensemble (Bendat & Piersol 1966).

The evolution of wave packet in the downstream direction is shown in figure 6. The amplitudes of the wave packets at different streamwise stations are magnified by different proportions for clarity; S, M and R indicate the mean separation, maximum-height and reattachment locations for the unexcited separation bubble respectively.

It can be seen that there is a low-frequency hump immediately following the wave packet reminiscent of the 'calmed regions' following turbulent spots (e.g. Ramesh, Hodson & Harvey 2001). Niew (1993) also observed such a hump in his separation-bubble experiments in the presence of impulsive forcing.

As pointed out by one of the referees, the evolution of the wave packet in the downstream direction can be divided into three regions: (1) the region upstream of the separation point consisting of a single oscillation cycle with mild growth and small dispersion; (2) the region from the separation point to just upstream of maximum height of the bubble with increased number of oscillations, larger growth of the disturbance (in fact exponential; see figure 7) and large dispersion; (3) the region

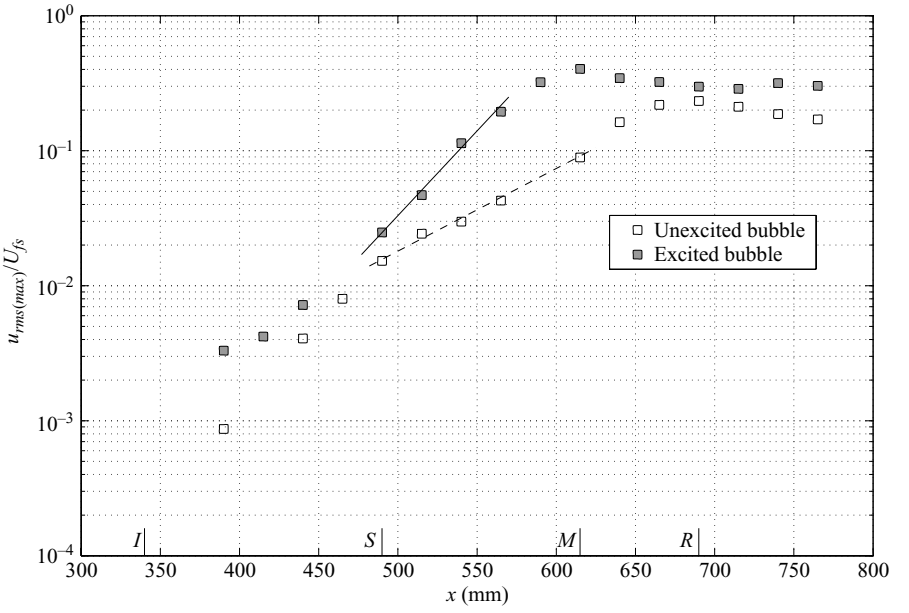

FIGURE 7. Semi-log plot of the disturbance amplitude (in form of r.m.s. intensity) for the excited and unexcited bubble; I is the location of introduction of disturbance; S is the separation point; M is the location of maximum height; R is the reattachment point; $U_{ref} = 2.78\,\mathrm{m\,s^{-1}}$.

downstream of the maximum-height location characterized by nonlinear breakdown and transition to turbulence. This is in conformity with the results of Marxen *et al.* (2003), who found the nonlinearity to set in just before the maximum-height location.

In the present case, the wave packet seems to be convectively unstable with respect to the location of disturbance introduction. Moreover, the convectively unstable disturbance in the attached boundary layer seems to retain this character even as it gets advected downstream through the separation region. That the separation bubble under consideration should be convectively unstable is entirely consistent with the theoretical studies on separation bubbles reported in the literature (e.g. Niew 1993; Alam & Sandham 2000). In these studies, it was found that absolute instability sets in for maximum reversed-flow values larger than about 15 % of the free-stream velocity. For the present case, the maximum backflow velocity has been estimated to be less than 8 % of the free-stream velocity (see § 5), and hence absolute instability is unlikely to occur.

In order to experimentally find out the absolute/convective nature of the disturbance in the separation bubble, an attempt was made to introduce the disturbance downstream of the separation location. However, this exercise was wholly unsuccessful in that the disturbance did not seem to grow downstream as long as it was introduced between the separation and the maximum-height locations. In other words, there is some 'lack of receptivity' inside the separation bubble in the dead-air region. There is some anecdotal support for this intriguing lack of receptivity from the work of other researchers also (Gaster 2005, private communication).

The streamwise variation of maximum ensemble-averaged r.m.s. fluctuating velocity is shown in figure 7. In the same plot, the corresponding distribution for the unexcited case is also shown for comparison. For the excited bubble, the presence of large growth of disturbances is seen in the initial portion of the bubble, upstream of the location of

maximum height. The disturbance amplitude reaches a maximum at the location of maximum height and decays further downstream. The amplification of disturbances is exponential, indicating that the stability characteristics of the separated shear layer can be explained using linear stability theory. This result is consistent with the findings of Dovgal *et al.* (1994), Watmuff (1999) and Marxen *et al.* (2003).

5. Inflectional instability mechanism in the primary stage of transition

The laminar mean profile between two parallel streams with respective velocities U_1 and U_2, where $U_2 > U_1$, is usually modelled by a hyperbolic-tangent velocity profile (Michalke 1964). With different levels of approximation of this mean profile (for enabling ease of analysis) such as a vortex sheet, piecewise linear profile and the full tangent profile, the stability of this flow has been very well studied in the literature. In this section, we study in detail the inflectional instability of the bubble. We also examine the conventional wisdom regarding separation-bubble transition that it is an inviscid instability phenomenon similar to the Kelvin–Helmholtz instability between two parallel streams.

Dovgal *et al.* (1994) performed linear stability analysis for velocity profiles with flow reversal close to the wall. Towards this, they modelled the mean velocity profile as

$$U(y) = [\tanh(a(y-d)) + \tanh(ad)]/[1 + \tanh(ad)] + b\sqrt{3}\eta\exp[-1.5\eta^2 + 0.5], \quad (5.1)$$

where $\eta = y/d$; b is a measure of the magnitude of reversed flow; and d is the non-dimensional distance of the inflection point from the wall. Dovgal *et al.* (1994) have used momentum thickness θ for normalization of y and d. For our purpose, we have used their analytical profile in a slightly modified form; while the same functional form has been used by us, the distance of inflection point from the wall y_{in} is used instead of momentum thickness for normalization, which fixes $d = 1$, and a and b are treated as free parameters. Using this modified expression, we seek a curve fit for the measured mean velocity profiles for performing linear stability analysis. It should be remembered though that the stationary hot-wire measurements close to the wall are fraught with uncertainty due to flow reversal. However, this is not expected to be a serious issue for fitting the analytical curves, as we make use of (5.1) for locations upstream of and at separation ($x \leqslant 490$ mm), where there is no flow reversal, and at a few downstream locations in the initial constant-pressure region ($x = 515$ mm to $x = 615$ mm) in which the flow reversal is small. Even for the case with small flow reversal, the curve-fit parameters are judiciously chosen so as to concur with the measured values away from the wall, and the expectation is that the trend close to the wall suggested by the analytical fit is realistic. This expectation is borne out by figure 8 with good correspondence between the analytical fits and the measurements at stations from $x = 415$ mm to $x = 615$ mm for $U_{ref} = 2.78\,\mathrm{m\,s^{-1}}$. The maximum reversed-flow velocity as given by the analytical fits is about 7.6 % at $x = 615$ mm, i.e. the location of maximum height. It may be noted that this is of the same order as the backflow measured by Watmuff (1999) using flying hot-wire anemometry. The same exercise (not shown here) has also been done for the higher reference speed, $U_{ref} = 5.4\,\mathrm{m\,s^{-1}}$.

The variation of integral quantities such as displacement thickness (δ^*), momentum thickness (θ) and shape factor ($H = \delta^*/\theta$) for the velocity profiles shown in figure 8 is plotted in figure 9. These quantities have been calculated using the fitted analytical profiles, since the measured profiles are expected to give erroneous results downstream

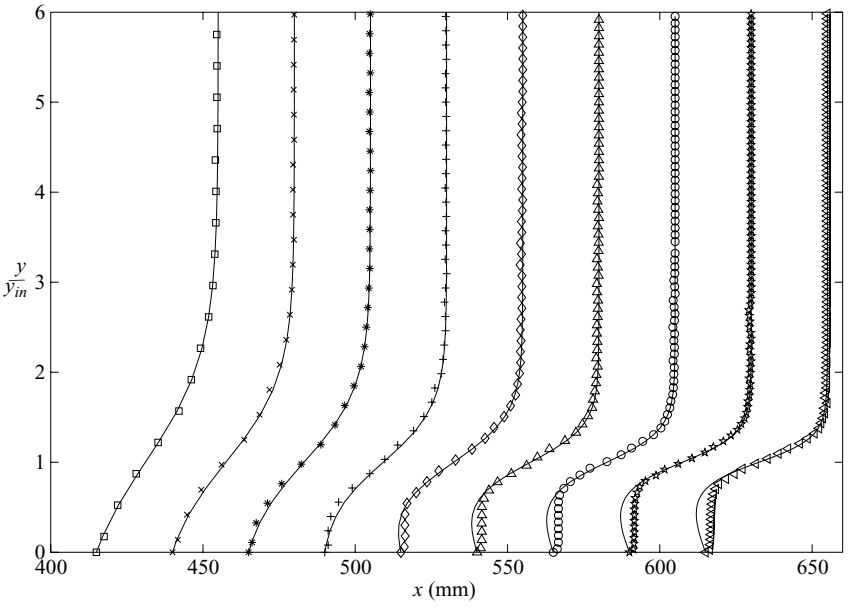

FIGURE 8. Measured mean velocity profiles (symbols) at streamwise locations: $x = 415$ mm to $x = 615$ mm and the analytical curve fits (continuous lines) due to Dovgal *et al.* (1994); $x = 490$ mm is the separation location; $U_{ref} = 2.78\,\mathrm{m\,s^{-1}}$.

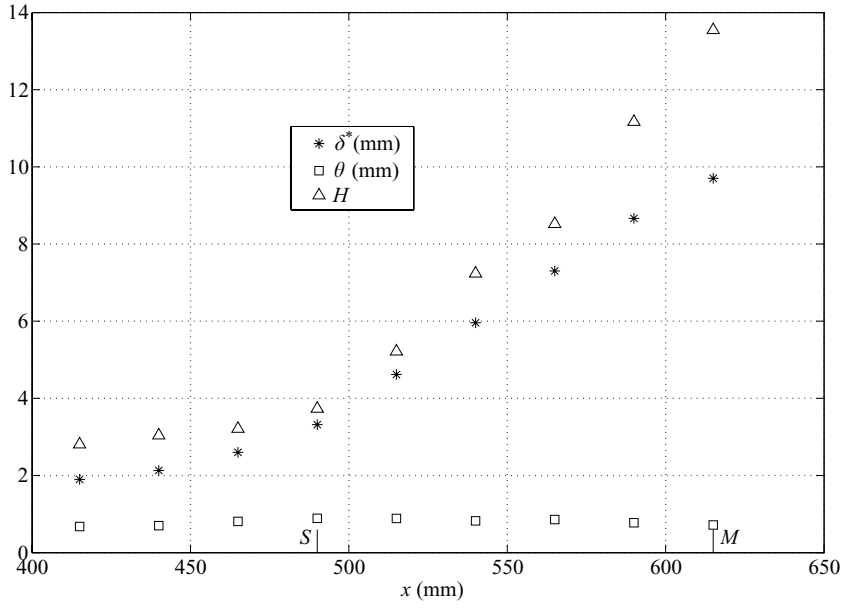

FIGURE 9. Variation of the integral parameters in the downstream direction; $U_{ref} = 2.78\,\mathrm{m\,s^{-1}}$; S and M indicate the separation and maximum-height locations respectively.

of separation as a result of the rectification of mean velocity in the reversed-flow region. The trends are in favourable agreement with the results reported in the literature (Fitzgerald & Mueller 1990; Haggmark *et al.* 2000; Lang, Rist & Wagner 2004). The Reynolds numbers based on the momentum thickness and the free-stream

velocity at the separation point ($Re_{\theta s}$) were calculated to be 322 for $U_{ref} = 2.78\,\mathrm{m\,s^{-1}}$ and 454 for $U_{ref} = 5.4\,\mathrm{m\,s^{-1}}$. These values are consistent with the figures obtained by: (i) Watmuff (1999), $Re_{\theta s} = 387$; (ii) Marxen *et al.* (2003), $Re_{\theta s} = 320$; (iii) Haggmark *et al.* (2000), $Re_{\theta_s} = 417$; and (iv) Gaster (1967), $Re_{\theta s}$ ranging from 136 to 432.

For performing the linear stability analysis, we have made use of an Orr–Sommerfeld code provided to us by Professor Gaster. We have also performed an inviscid stability analysis by numerically solving the Rayleigh equation (by using a code developed in-house) for comparison.

In the literature the expression for the most amplified frequency (of the hyperbolic-tangent velocity profile) is given by the non-dimensional form as $\omega^* = (1/4)\delta_\omega 2\pi f/U_m = \text{constant}$, for a given value of the velocity ratio $\lambda = \Delta U/(2U_m)$. Here, the dimensional frequency is f, the velocity difference across the shear layer $\Delta U = U_2 - U_1$, the average velocity $U_m = (U_1 + U_2)/2$ and the so-called vorticity thickness $\delta_\omega = \Delta U/(\partial U/\partial y)_{max}$. This analysis was originally due to Monkewitz & Huerre (1982) who found ω^* to vary in the interval [0.222 0.21] when λ varies in the interval (0 1]. In other words, the analysis is strictly valid for co-flowing mixing layers only and not for a counter-current mixing layer. Even so, other workers (Pauley *et al.* 1990; Watmuff 1999) have found this scaling to apply near the maximum-height location of the separation bubble, and we will examine this later.

The Monkewitz & Huerre (1982) scaling for the most amplified frequency given above does not explicitly include the effect of an adjoining wall. The presence of a wall, as in the separation-bubble problem, would seem to have a tempering effect thereby modifying the most amplified frequency of the inflectional instability mechanism for free shear layers. In this connection, the conclusions of Betchov & Criminale (1967) seem relevant; they observed that the distance of the inflection point from the wall (y_{in}) is an important parameter in dictating the inflectional instability of wall-bounded flows. This is also supported by the results of Taghavi & Wazzan (1974), Nayfeh, Ragab & Masad (1990), Das (1998) and Boiko *et al.* (2002). The broad conclusion from all these works is that as the distance of the inflection point from the wall (y_{in}) is increased, the growth rates are also increased, and the mean velocity profile becomes more unstable. Das (1998) has plotted the results of a temporal stability analysis of an inflectional profile such as the variation of maximum growth rate against y_{in}. However, other researchers mentioned above have not explicitly used y_{in} as a parameter in their investigations. Recognizing its possibly important role in the inflectional instability dynamics, we set out to use y_{in} as a scaling parameter for the most amplified frequency. In view of this, we write the functional form of the most dominant frequency for a wall-bounded shear layer as $f = F(U_{in}, y_{in}, \nu, \delta_\omega)$, where U_{in} is the mean velocity at the inflection point and ν is the kinematic viscosity. Different non-dimensional groups can be constructed from this functional relationship, and the task is to choose the most relevant ones. In order to obtain the appropriate scaling principle and the correct functional dependence, we performed a spatial stability analysis of a piecewise linear profile adjoining a solid wall as an approximation to the mean velocity profile in a separation bubble. The details of the derivation are presented in Appendix B. The conclusion from this study is that the scaling principle for the most amplified frequency in the linear regime for an adverse-pressure-gradient boundary layer/separated flow is given by

$$\frac{f\left(y_{in}^2 + \delta_\omega^2\right)}{\nu} \sim \frac{U_{in}\, y_{in}}{\nu}\sqrt{\frac{y_{in}}{\delta_\omega}}. \tag{5.2}$$

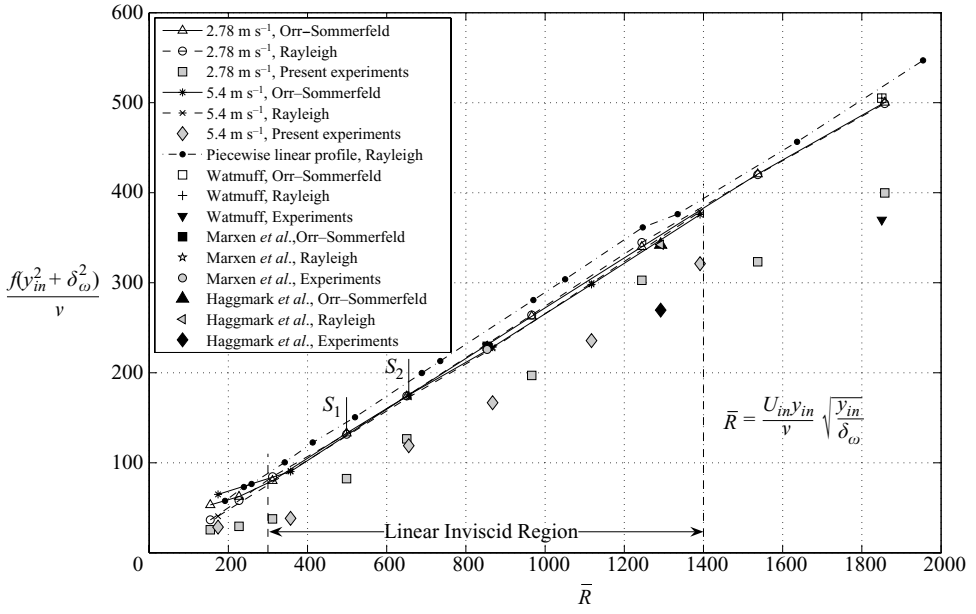

FIGURE 10. Scaling relation for the most amplified frequency in the separation bubble for both the reference speeds; S_1 indicates the separation location for $U_{ref} = 2.78\,\mathrm{m\,s^{-1}}$ and S_2 for $U_{ref} = 5.4\,\mathrm{m\,s^{-1}}$. Experimental and corresponding theoretical calculations for Watmuff (1999), Marxen *et al.* (2003) and Haggmark *et al.* (2000) are also shown.

In other words, the frequency is scaled with a viscous-diffusion scale (Villermaux 1998), and this is expected to vary like a modified Reynolds number given by $\overline{R} = (U_{in}\, y_{in}/\nu)\sqrt{y_{in}/\delta_\omega}$; the factor $\sqrt{y_{in}/\delta_\omega}$ is required so that the resulting functional form for the non-dimensional frequency is very nearly linear for the piecewise linear profile as explained in Appendix B.

The non-dimensional frequencies of the most amplified modes resulting from spatial stability calculations (using both the Orr–Sommerfeld and Rayleigh equations) are plotted in figure 10 along with the corresponding measurements for the excited case. This exercise has been done for the two different reference speeds, $U_{ref} = 2.78\,\mathrm{m\,s^{-1}}$ and $U_{ref} = 5.4\,\mathrm{m\,s^{-1}}$. The results from the stability analysis of the piecewise linear profile (suitably modified for the choice of variables, U_{in} and y_{in}) are also indicated in the same plot. The variations of y_{in} (mm), δ_ω (mm) and f (Hz) with the streamwise coordinate x (mm) are discussed in Appendix C and they further justify the particular form of the scaling parameters given above.

It can be seen from figure 10 that the curves of the Orr–Sommerfeld and Rayleigh calculations for the most amplified frequency are very nearly identical for both the reference speeds and can be approximated by a linear variation in the region between $\overline{R} = 300$–1400. These points correspond to the streamwise locations starting approximately from $x = 460\,\mathrm{mm}$ (i.e. upstream of separation) all the way downstream to the end of the linear regime of disturbance growth. The experimental points for both the reference speeds collapse well onto to each other to display a single trend and lie very close to the theoretical curves – nearly parallel to them with a slightly different slope (with a small offset). This offset between the theoretical and experimental trends for the most amplified frequency seen in figure 10 needs to be clarified. Note that the non-dimensional frequency obtained from experiment is lower roughly by a factor of

1.2 compared to theory (especially close to and downstream of the separation point). In this connection, the observation of Zaman & Hussain (1981) is relevant. They found that the most amplified frequency in a mixing-layer experiment was 1.4 times smaller than the corresponding prediction from linear stability theory. We speculate this difference might be due to the fact that what is observed in experiment is in fact the result of an integrated growth rate over a certain streamwise extent, whereas linear stability theory (the Orr–Sommerfeld and Rayleigh equations) yields a mode with a frequency which is dominant at that location (where only a local growth rate would have mattered). Zaman & Hussain (1981) had also offered a similar reasoning to explain the systematic shift of the experimental points below the theoretical curve by a constant factor. In consideration of this aspect, we conclude that the agreement between theory and experiments shown in figure 10 is good.

Two points are worth noting in connection with the agreement between experiments and theory in figure 10. First of all, there is a systematic departure of the experimental points beyond $\overline{R} = 1400$. This corresponds to the point close to the mean maximum height of the bubble at which we have already seen that the nonlinear regime starts. Secondly, below $\overline{R} = 300$, the experimental points again move away from the linear trend as we move upstream. The calculations resulting from Orr–Sommerfeld equation also display a trend (for both the reference speeds) similar to that of the experimental points in this range. Moreover, for $\overline{R} < 300$, the Orr–Sommerfeld calculations are slightly different from the Rayleigh calculations for both the reference speeds. For $\overline{R} > 300$, the theoretical curves for the most amplified frequency from the Rayleigh and Orr–Sommerfeld linear stability theories collapse onto one another as seen in figure 10. It is well known from the literature (see Hammond & Redekopp 1998; Healey 1998) that for wall-bounded inflectional profiles, the Orr–Sommerfeld equation yields both inflectional (inviscid) and wall (viscous) modes. On the other hand, the Rayleigh equation gives rise to only inflectional (inviscid) modes. The fact that both the curves collapse for $\overline{R} > 300$ in figure 10 means that the essential instability dynamics of the bubble is inviscid in character. This is of course understandable, as the instability of the inflection point is the primary focus here. It is noteworthy that this instability can be traced back to the attached boundary layer upstream of separation (up to $x = 460$ mm) consistent with our expectations outlined earlier. More specifically, we have already noted that the inflectional instability of the upstream boundary layer is convective in nature, and as a result it is being advected downstream of the separation location. Hence figure 6 in conjunction with figure 10 suggests that the inflectional instability does indeed originate upstream of the separation location, and it is advected downstream to manifest as the inviscid instability of the inflectional profile associated with the separation bubble. It is striking to note that the variation of trends in both amplitude (in figure 6) and frequency (figure 10) of the disturbance are continuous across the separation zone, presumably indicative of the same instability mechanism at work upstream and downstream of the separation location.

The collapse of the theoretical curves for two different reference speeds indicates that the scaling principle for the most amplified frequency, introduced in the present work, is fundamentally correct. In order to demonstrate the universality of this scaling principle, we have performed linear stability analyses of the mean velocity profile measurements of Watmuff (1999), Haggmark *et al.* (2000) and Marxen *et al.* (2003) upstream of the maximum-height location – at $x = 800$ mm, $x = 840$ mm and $x = 250$ mm in Watmuff (1999), Haggmark *et al.* (2000) and Marxen *et al.* (2003) respectively, and these are also shown in figure 10. It can be seen that there is excellent agreement between the Rayleigh and Orr–Sommerfeld calculations based

on the mean velocity profiles measured by the above authors and those based on our experiments using the analytical curve fit. This demonstrates the soundness of the scaling principle as well as its universality. (This agreement also vindicates the goodness of the analytical curve fits as used here.) The experimental points of Watmuff (1999) and Haggmark *et al.* (2000) display an offset similar to those of the present work. This is because the former uses an impulsive forcing, and in the latter, transition is triggered by the natural disturbance field which is of a broadband nature. In both these cases it is conceivable that the actual transition is effected by a selected band of unstable frequencies (Gaster & Grant 1975) as in the present experiments. On the other hand, the measured frequency of Marxen *et al.* (2003) agrees very well with the theoretical frequency and does not display any offset. This is so because their experiment used harmonic forcing wherein the integrated growth rate is likely to be the same as the local growth rate. Furthermore, the data point from the work of Watmuff (1999) presumably lies at the end of the linear regime, and hence the departures from linear trends start there. Indeed a careful look at figure 9 in Watmuff (1999) does show that this streamwise location at which the most amplified frequency is reported by him lies very nearly at the beginning of the nonlinear regime in his experiment (roughly $x = 790$ mm in Watmuff 1999). Finally, the results from piecewise linear profile (included in figure 10) are also in good agreement with the other predictions, confirming the universality of the proposed scaling, independent of the precise form of the mean velocity profile.

The success of the scaling $f(y_{in}^2 + \delta_\omega^2)/\nu \sim (U_{in}\, y_{in}/\nu)\sqrt{y_{in}/\delta_\omega}$ demonstrated above means that we can rewrite this to express the most amplified frequency as $f \sim U_{in}/\overline{L}$, where $\overline{L} = ((y_{in}^2 + \delta_\omega^2)/y_{in})\sqrt{\delta_\omega/y_{in}}$. In other words, this can be interpreted as a convective scaling for the frequency wherein the length scale $\overline{L}$ is a composite length scale which takes into account both the inflection-point height and the vorticity thickness simultaneously. For a non-zero value of δ_ω, we get the physically plausible result $f \to 0$ as $y_{in} \to 0$.

We had raised the question of applicability of the scaling of Monkewitz & Huerre (1982) to the separation-bubble problem. As mentioned before, Pauley *et al.* (1990) and Watmuff (1999) applied this scaling to the case of separation bubble; they took $\omega^* \approx 0.21$ for calculating the most amplified frequency. They found this to agree with the dominant frequency observed slightly upstream of the maximum-height location of the bubble. We also have applied the Monkewitz & Huerre (1982) scaling to the present results. For the boundary layer upstream of separation, this was relatively straightforward, as there are no uncertainties. However, downstream of separation, since there are measurement uncertainties due to the presence of reversed flow, we could not estimate the vorticity thickness and the maximum reversed-flow velocity from our single-wire measurements. We have instead made use of the analytical fits as shown in figure 8 which are expected to give fairly good estimate of these quantities. Using these estimates, the results of our experimental and theoretical studies for the most amplified frequency are plotted using the Monkewitz & Huerre (1982) scaling as shown in figure 11. It is observed that the theoretical non-dimensional frequency (from both the Orr–Sommerfeld and Rayleigh calculations) crosses the value of $\omega^* = 0.21$ close to the maximum-height location, whereas the experimental frequency is slightly below this value. The systematic shift again can be attributed to the reasons already discussed – difference between the integrated and local growth rates. It is interesting to note that as we move well inside the separation-bubble region, the agreement of this scaling with the experiments gets better which is consistent with the observation

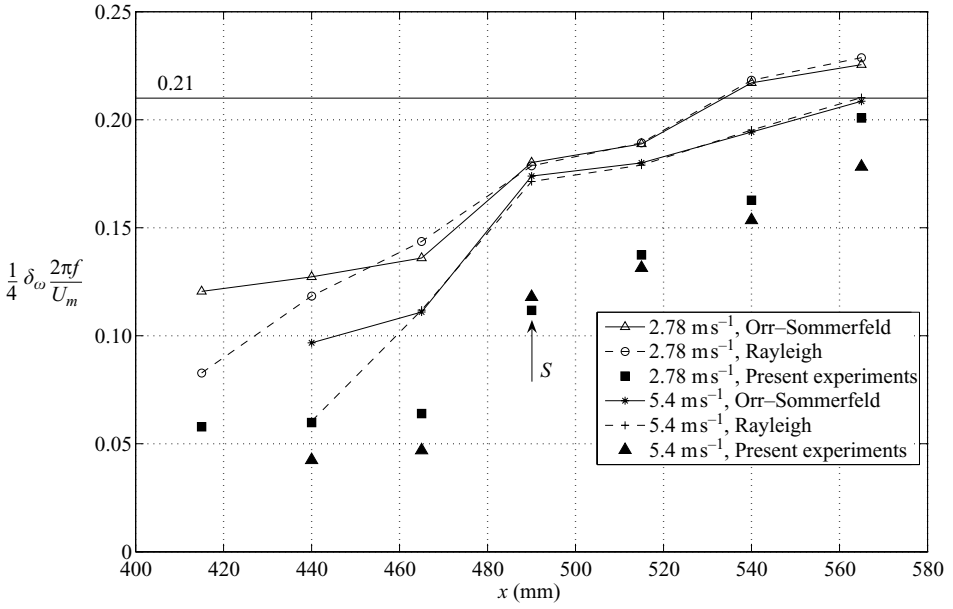

FIGURE 11. Variation of the non-dimensional frequency based on vorticity thickness (Monkewitz & Huerre scaling) with streamwise distance x.

of Watmuff (1999). However, it is clear from figure 11 that the agreement between experiments and the Monkewitz & Huerre (1982) scaling (i.e. $\omega^* = 0.21$) becomes less compelling as we move upstream towards the separation point. As we move upstream of separation, the agreement is altogether weak. As discussed earlier, this disagreement is primarily due to the absence of wall-proximity effects in this scaling which is based on vorticity thickness alone.

Hence we can conclude that the wall-proximity effect is an important ingredient needed to capture the correct scaling principle for the most amplified frequency in a wall-bounded flow; and since this effect weakens as the separated shear layer progressively moves away from the wall, there is better agreement with the $\omega^* = 0.21$ scaling near the maximum-bubble-height location. However, it must be noted that the value $\omega^* = 0.21$ corresponding to the Monkewitz & Huerre (1982) scaling for the (hyperbolic-tangent) free shear layer is reached only for one streamwise location upstream of maximum height. This is seen in Watmuff (1999) as well. We contend it may not be appropriate to conclude from such a one-point match that the instability of the separated shear layer is similar, in all respects, to that of the free shear layer. Rist, Maucher & Wagner (1996) have done linear stability analysis to assess the influence of wall on the inflectional instability. They found that the distance of the inflection point from the wall needed to turn the mean velocity profile in the bubble into the free shear layer profile was rather large. They also remarked that the direct comparison between a separated shear layer and a free shear layer should be regarded with some circumspection. In view of these, the scaling proposed in the present work, which takes into account aspects of both the free shear layer dynamics and the wall-proximity effect, is clearly seen to be more appropriate and effective, for the separation-bubble problem, than the Monkewitz & Huerre (1982) scaling.

Next, the production of disturbance kinetic energy $-\overline{u'v'}\partial U/\partial y$ (with the constant density term scaled out) obtained from the linear stability calculations is plotted in

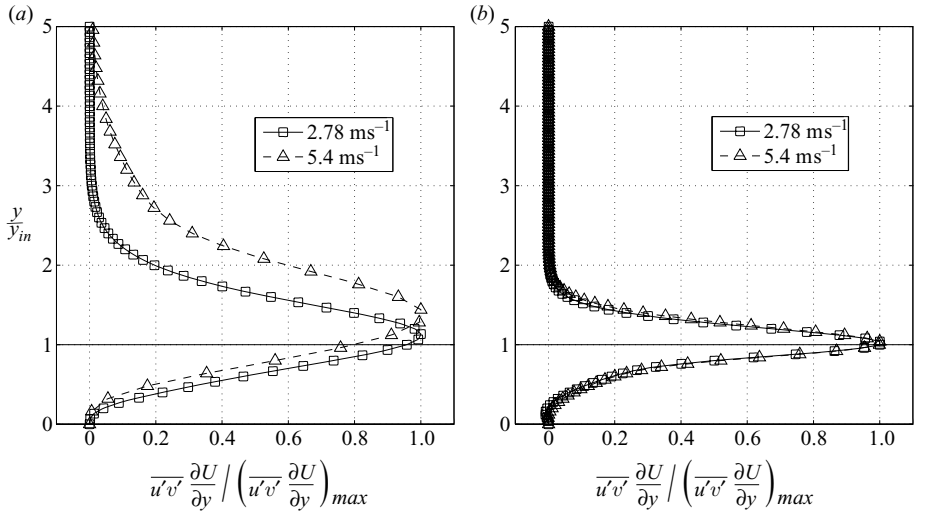

FIGURE 12. Distribution of normalized production of disturbance energy (for the most amplified modes) for the streamwise location (*a*) upstream of separation, $x = 415$ mm, and (*b*) downstream of separation, $x = 515$ mm.

figure 12 for the most amplified waves. Here u' and v' are the disturbance streamwise and cross-stream velocities and $\partial U/\partial y$ is the mean velocity gradient. These are reported here for two different streamwise locations – one upstream of separation and the other downstream. It can be easily seen that the wall-normal location at which peak production occurs moves closer to the inflection point as the separation bubble is approached from the upstream adverse-pressure-gradient region.

The point has already been made in connection with figure 10 that there is a departure in trends between the curves of most amplified frequency obtained by the Rayleigh and Orr–Sommerfeld calculations for $\overline{R} = (U_{in}\, y_{in}/\nu)\sqrt{y_{in}/\delta_\omega} < 300$. This suggests that for $\overline{R} < 300$ (and correspondingly $x < 460$ mm), the Rayleigh (inviscid) instability calculation is inadequate to capture the transition dynamics in the attached adverse-pressure-gradient boundary layer well upstream of separation. This is because the viscous effects are relatively stronger there, perhaps because of the dominance of the wall mode of instability (i.e. TS mechanism). For $x < 460$ mm, where the viscous effects are expected to be important, the mean velocity gradient near the wall is larger (compared to that near separation at which it almost vanishes), thereby resulting in an increased transfer of energy to the wall mode from the mean flow. In other words, the relative importance of viscous instability mechanism (such as due to the wall mode) in comparison to the instability associated with the inflectional mode changes its character as we move downstream towards separation. In order to see this clearly, we plot the ratio y_{in}/y_{max} against the streamwise distance (x) in figure 13 for the most amplified modes; y_{max} is the wall-normal distance at which the production peaks and y_{in} is the wall-normal distance at which the inflectional point of the mean velocity profile is located (as already mentioned before), at a given streamwise station.

The ratio (y_{in}/y_{max}) could be usefully interpreted as a measure of the relative importance of the inflectional and wall modes. If this ratio is small compared to unity it means the wall mode is stronger, whereas if the ratio approaches unity the inflectional mode controls the disturbance dynamics, and the wall mode becomes relatively weak. For a zero-pressure-gradient laminar boundary layer (Blasius profile),

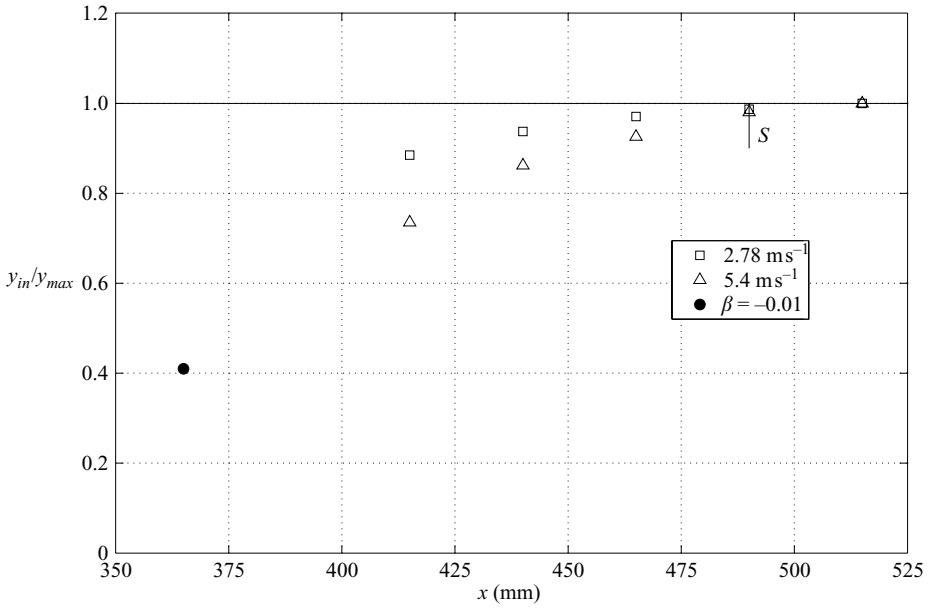

FIGURE 13. Variation of the ratio of location of inflection point to the location of production maximum (indicating relative importance of inflectional and wall modes) with streamwise distance, for the most amplified waves. Also included is the data for Falkner–Skan pressure gradient parameter $\beta = -0.01$ (weak inflectionality) for comparison.

this ratio is 0 (since $y_{in} = 0$ in this case), and for a separated profile dominated by inflectional instability, this ratio can be expected to assume a value of 1. It can be seen in figure 13 that this is indeed the case: to start with the wall mode is relatively stronger (when the local Reynolds number is also low), but as we move downstream towards the separation location, the inflectional mode becomes progressively more important and influential. Downstream of the separation location, the inflectional mode dominates the instability dynamics. A data point for the Falkner–Skan profile with $\beta = -0.01$ is also plotted in figure 13 for the sake of comparison. The inflection point for this profile is very close to the wall, and therefore the instability dynamics can be expected to be predominantly viscous (wall mode type). As a result the ratio y_{in}/y_{max} is much less than 1 (as compared to the present experimental points), showing the usefulness of this ratio in characterizing the dominant instability mechanism.

The smooth switch-over of the dominant instability mechanism from the wall mode to the inflectional mode (as discussed above), as the separation point is approached, can be further illustrated by considering the evolution of disturbance mode shapes with downstream distance. A carpet plot of the distribution of amplitude and phase of u' and v' perturbations (for the most amplified frequency) obtained by solving Orr–Sommerfeld equation for various locations across the separation point is shown in figure 14(a–d) for $U_{ref} = 2.78\,\mathrm{m\,s^{-1}}$. At $x = 415\,\mathrm{mm}$ (which is well upstream of the separation point, $x = 490\,\mathrm{mm}$), the mode shapes look similar to those typical of viscous instability (wall mode type) with u' amplitude peaking close to the wall and close to the boundary-layer edge with no peak at the inflection point. This is consistent with the value of y_{in}/y_{max} being less than 1 at this station as in figure 13.

As we move towards the separation point, the mode shapes get modified progressively and are gradually transformed into the ones typical of inflectional

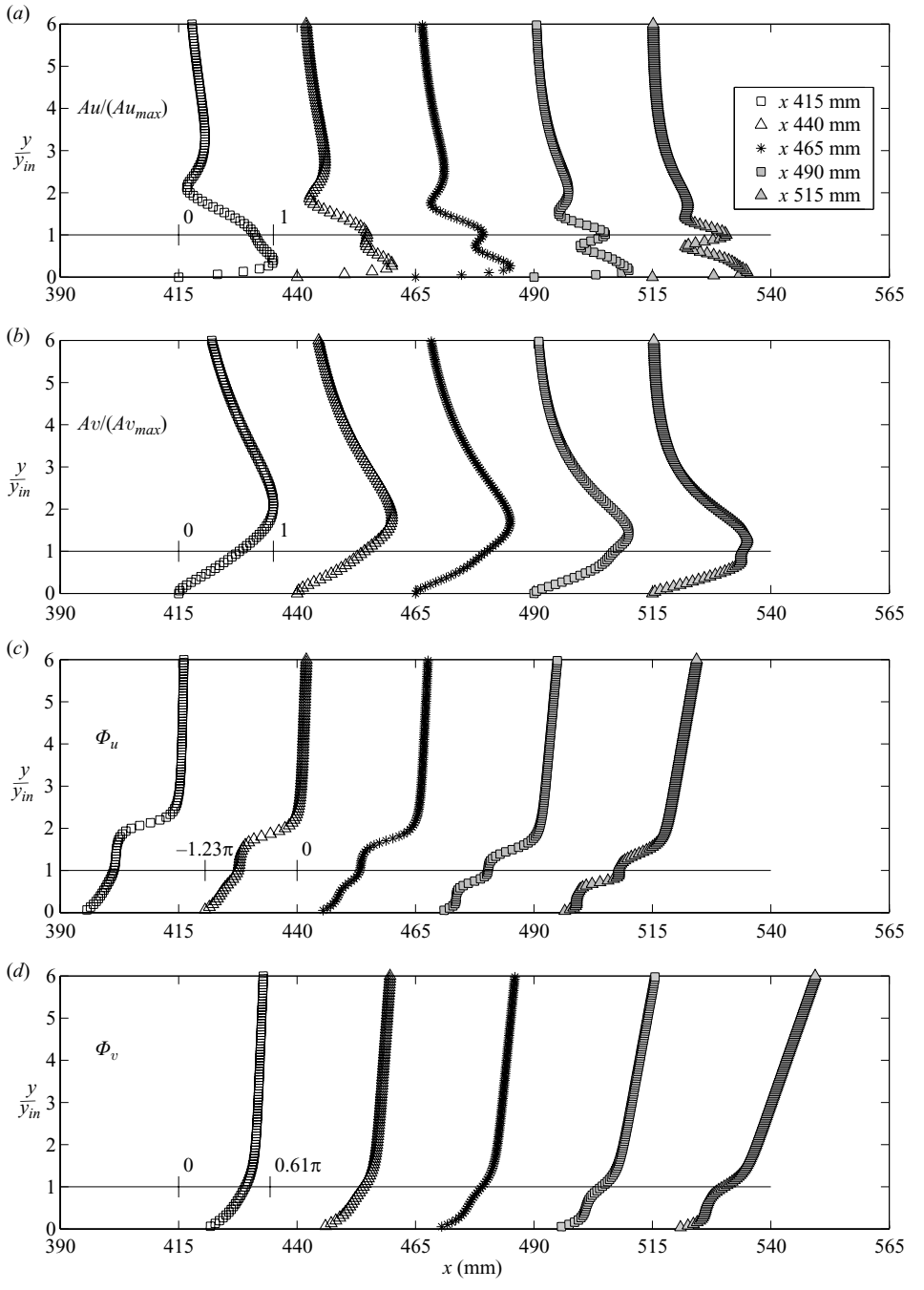

FIGURE 14. A carpet plot showing distribution of (*a*) u' amplitude (A_u), (*b*) v' amplitude (A_v), (*c*) u' phase (Φ_u) and (*d*) v' phase (Φ_v) for different streamwise locations from well upstream of separation to a little downstream of it, for the most amplified waves; $U_{ref} = 2.78\,\mathrm{m\,s^{-1}}$.

instability (see Haggmark *et al.* 2000). This is more dramatically seen in figure 14(*a*), where a distinct peak emerges at the inflection point in the u' amplitude distribution at $x = 465\,\mathrm{mm}$ and gets stronger compared to the peak close to the wall at and

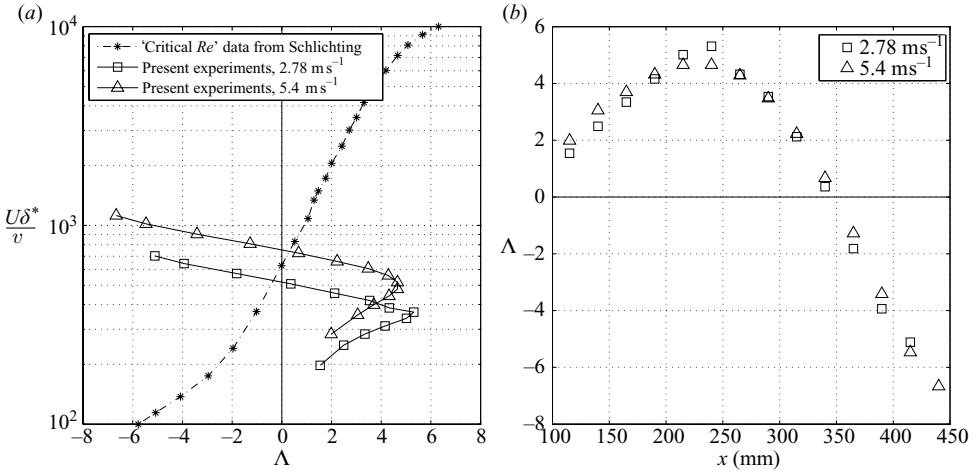

FIGURE 15. (*a*) Plot of Reynolds number against Pohlhausen parameter (Λ) along with the critical Reynolds number data (from Schlichting 1960). (*b*) Variation of Λ with the streamwise distance x.

downstream of the separation point. Furthermore, figure 13 shows that at this streamwise location (upstream of separation), the maximum production occurs very close to the location of inflection point. Both these results convincingly support our contention that the inflectional instability of the separation bubble originates from the upstream attached boundary layer and is advected downstream of separation as a result of the convective nature of instability (as already discussed with reference to figure 6). Moreover, the mode shapes at $x = 515$ mm, which is downstream of separation location, are seen to be in qualitative agreement with the laser Doppler anemometry measurements of Marxen *et al.* (2003) establishing the basic soundness of the present analysis.

So far, we have exclusively focused on the adverse-pressure-gradient region upstream of separation and the separation-bubble region, to decide on the nature of the transition mechanism. For this to be meaningful, we have to rule out the role of any TS mode which might have been initiated in the favourable-pressure-gradient region upstream of the peak-suction location. Towards this, we ask the question: at what streamwise location does the flow in the boundary layer become critical? In order to pinpoint the approximate streamwise station at which the instability sets in and the flow becomes critical, we plot the variation of the critical Reynolds number (based on displacement thickness) as a function of the Pohlhausen parameter ($\Lambda = (\delta^2/\nu)(\mathrm{d}U_{fs}/\mathrm{d}x)$, where δ and $\mathrm{d}U_{fs}/\mathrm{d}x$ are the boundary-layer thickness and the streamwise velocity gradient of the free-stream velocity respectively) in figure 15, as correlated by Schlichting (1960). In the same figure we also plot the variation of the local Reynolds number (based on displacement thickness) starting from the favourable-pressure-gradient region all the way to the adverse-pressure-gradient region in our experiments. The point at which these two curves cross is the point of onset of instability, and it can be seen to be lying close to the peak-suction location at which $\Lambda = 0$ (figure 15*a*). For $U_{ref} = 2.78\,\mathrm{m\,s^{-1}}$, the crossover is slightly downstream of the peak-suction location, whereas for $U_{ref} = 5.4\,\mathrm{m\,s^{-1}}$, it is slightly upstream. Figure 15(*b*) shows the variation of the Polhausen parameter with streamwise distance in the present experiments. From this plot, the location at which $\Lambda = 0$ can be identified

to be at $x = 345$ mm. In other words, the location of instability onset is very close to this station. Hence the possibility of the upstream favourable-pressure-gradient region taking part in the transition dynamics can be ruled out. It must be noted that we are resorting to this approximate integral method to locate the critical location, because we do not have detailed boundary-layer measurements upstream of peak suction, i.e. in the favourable-pressure-gradient region.

The summary from this section is that the instability associated with the separated region is indeed primarily inviscid in character. The seeds of this inflectional inviscid instability can be traced back to the upstream attached boundary layer, where there is an inviscid instability associated with the inflectional velocity profile. This is convectively unstable and hence is advected downstream to the separation-bubble region. For the streamwise extent starting slightly upstream of separation and extending very nearly up to the end of the dead-air region in the bubble, the instability dynamics are dictated by a linear inviscid mechanism. For this region, we have proposed a new scaling principle for the most amplified frequency by taking wall-proximity effects into account. Downstream of separation, at some location close to the maximum bubble height, the shear layer would have moved sufficiently far away from the wall. For this case, the disturbance dynamics become nearly indistinguishable from the free shear layer instability of the classical type, so that it may be describable by the Kelvin–Helmholtz instability paradigm (as seen from figure 11). Around this maximum-height location, the inception of nonlinearity is likely to take place. In this connection, reference may be made to Maucher, Rist & Wagner (1999) and Marxen *et al.* (2003), who have shown that there could be an onset of secondary absolute instability close to the mean maximum height of the bubble (provided the intensity of reversed flow exceeds some threshold), and this is a precursor to the eventual nonlinear evolution of the instability before turbulent reattachment.

It must be mentioned that all the results stated above have been obtained through linear stability analysis with local parallel assumption. However, the flow domain involving the separation bubble could be expected to be non-parallel, and the utility of the parallel-flow analysis, as used in the present study, is called to question. Boiko *et al.* (2002) have discussed this issue in some detail. Comparing the instability characteristics obtained from parallel theory with DNS and experiments, they found that the agreement amongst them was quite good. Marxen *et al.* (2003) also found a good agreement between the parallel theory and the DNS. Comparison of non-local stability analyses and the Orr–Sommerfeld results of Theofilis, Hein & Dallmann (2000) further supports this observation. The reasons for the success of parallel linear stability theory in what could be expected to be an evolving and therefore non-parallel flow is not clear. It is something of a paradox and not yet completely understood as Boiko *et al.* (2002) note. Our simple justification for using the parallel theory derives in view of this and in any case as a starting point for future investigations with non-parallel theory.

6. Discussion

A clear picture is beginning to emerge as to how linear instability mechanism is initiated in a separation bubble. The inflectional instability associated with the separation bubble is seen to have its origins upstream of the separation in the attached-boundary-layer region. At the point of onset, this inflectional instability is not strong, and the wall mode connected with the TS mechanism appears to be the stronger one. Downstream in the attached boundary layer, the mean velocity gradient

near the wall which feeds the wall mode progressively becomes weaker. At the same time the inflection point moves away from the wall sufficiently, for the inflectional mode to become stronger.

For $\overline{R} > 300$, the collapse of the Orr–Sommerfeld and Rayleigh calculations in figure 10 suggests that the dynamics are inviscid in that region. Moreover, the inflectional instability mode is also convectively unstable and hence is advected downstream into the separation region. Finally, when the separated shear layer has moved away sufficiently far from the wall, the instability of the inflectional mode assumes the characteristics of classical Kelvin–Helmholtz mechanism at some location just upstream of the maximum bubble height. Presumably, this must be triggering some form of secondary instability, and this has been found to be absolutely unstable by Marxen *et al.* (2003) if the backflow is sufficiently strong. This is a precursor to the nonlinear instability of the disturbance before the final turbulent reattachment. It has already been commented in § 5 that the streamwise location ($x = 800$ mm) for which Watmuff (1999) has reported good agreement between the measured most amplified frequency with the scaling $\omega^* = 0.21$ lies at the end of the linear regime and at the beginning of the nonlinear regime. In this streamwise region (see figure 14 in Watmuff 1999), he has also found the spanwise vorticity contours displaying a cat's-eye pattern. While this has been attributed to the linear Kelvin–Helmholtz instability mechanism in his work, it could as well have been a manifestation of nonlinearity. In this connection, it is interesting to note that the presence of the cat's-eye pattern is associated with both the linear and nonlinear instability regimes (Maslowe 1986).

If as argued, the inflectional instability originates upstream of the separation location, will there be no laminar–turbulent transition if the oncoming flow is somehow kept very clean or if the inflectionality is very weak? The answer to this question has to be a qualified yes. If the inflectional instability is weak, its propensity to accentuate disturbances is weak. In that case, the flow could stay laminar even downstream of separation. A case in point is the separated flow behind a backward-facing step when the step height is very small. For this case, inflectionality of the profile downstream of separation is presumably very weak, as the inflection point is very close to the wall, and hence does not succeed in destabilizing and transitioning the flow. Examples of this could be seen in the experiments of Eaton & Johnston (1980) and Sinha, Gupta & Oberai (1981). Dovgal *et al.* (1994) presented experimental results for flow over a rectangular hump on a flat plate (figure 28 in their paper); the TS wave of the upstream attached boundary layer is seen to transform into eigensolutions of the separation profile and to change gradually in the downstream direction before reverting to TS wave distribution after the flow reattaches laminarly. In this case, we can attribute the relative weakness of the inflectional point and the associated instability, for not being effective in transitioning the separation profile. Another example of laminar reattachment is the flow visualization of Werle done at the Office National d'Etudes et de Recherches Arospatiales (ONERA), documented by VanDyke (1982) in his album of fluid motion (plate 35). It shows a leading-edge separation on a 2 % thick flat plate (with bevelled edges) inclined at 2.5° to the free stream at a Reynolds number of 10 000. This is relatively low-Reynolds-number separation, but the essential point to note is that the inflection point is likely to be very close to the wall, and therefore it is not strong enough to incite unstable waves to cause transition. The flow situations cited involving laminar-flow reattachment show that these are instances in which even if there is an upstream disturbance present,

the flow in the separated region stays laminar, unless the inflection point moves sufficiently away from the wall. This implies that the strength of the inflection point as well as the amplitude of free-stream disturbance together decide whether transition will take place in the separated shear layer.

Another way by which transition can be effected has been suggested by Spalart & Strelets (2000). According to this picture, if the upstream flow is kept clean, the flow could still become turbulent by a mechanism that they call 'transition by contact' – the 'backwaters', as it were, from the region downstream of turbulent reattachment move upstream to contaminate and transition the flow. But the picture is speculative at this stage, and it is not clear under what conditions this mechanism is likely to be at play.

In all of the above, the evolution of two-dimensional disturbance waves has been considered especially up to the end of the linear stability regime. This is of course a reasonable supposition in the front portion of the bubble up to the end of the dead-air region (see figure 5). In view of the result of Marxen *et al.* (2003), we can expect three-dimensional disturbances to be unimportant in the linear regime. We plan to study the evolution of disturbances in the nonlinear regime and the route to reattachment as part of a future investigation.

7. Conclusions

A detailed experimental and theoretical investigation of the linear instability mechanisms associated with a laminar separation bubble has been performed. It has been shown that the primary instability mechanism in a separation bubble, in the form of two-dimensional waves, is inviscid inflectional in nature, and its origin can be traced back to the region upstream of separation. In other words, the inviscid inflectional instability associated with the separated shear layer should be logically seen as an extension of the instability of the upstream attached adverse-pressure-gradient boundary layer. This modifies the traditional view that connects the origin of the inviscid instability in a bubble to the detached shear layer outside the bubble with its associated Kelvin–Helmholtz mechanism. We have also obtained a scaling principle for the most amplified frequency in terms of the height of the inflection point from the wall (y_{in}) and the vorticity thickness (δ_ω) and shown it to be universal, independent of the precise shape of the velocity profile. This was motivated by the linear inviscid spatial stability analysis of a piecewise linear profile adjoining a solid wall. We have shown that only when the separated shear layer has moved considerably away from the wall (and this happens near the maximum-height location of the mean bubble), a description by the Kelvin–Helmholtz instability paradigm, with its associated scaling principles (such as $\omega^* = 0.21$), could become relevant.

We would like to thank the Indian Aeronautical Research & Development Board (Aerodynamics Panel) for financial support through a sponsored project for the initial part of the present study. Thanks are due to Professor Mike Gaster for lending us his stability code and for various discussions. We record our sincere thanks to Professor R. Narasimha and Professor K. R. Sreenivasan for going through an earlier version of this draft and making suggestions. We would also like to thank the referees who have made many useful suggestions for improving the quality of the paper.

Appendix A. Three-dimensionality of the mean flow

In this appendix, we briefly address the issues of three-dimensionality of the mean flow close to the wall, associated with the bubble, and the justification for using centreline hot-wire measurements in the present work. The surface flow-visualization technique (mentioned in § 3), first reported by Langston & Boyle (1982) that we refer to as the 'ink-dot-matrix' method, has been used to obtain surface-streamline patterns covering almost the entire width of the test section. This method involves the use of a shear-sensitive tracer on the surface of the flat plate, which when acted upon by the flow, leaves behind a surface-streamline pattern. In the current study, a matrix of ink dots using a permanent marker pen (Staedtler Lumocolor 318) was made on a sheet of artist's tracing paper. A fine layer of methyl salicylate ($C_8H_8O_3$) was sprayed on the paper, which was then stuck on to the flat plate using a very thin adhesive tape. The chemical spray dissolves the ink dots, turning them into tiny sources of ink on the surface of the plate itself. Due to the surface shear imposed by the oncoming flow, the ink moves in the direction of flow, thereby leaving behind a pattern of comet-like streaks on the surface. The streak emanating from each dot, thus, points towards the direction of local time-averaged skin friction (and therefore local surface streamline). It must be noted that this method gives a sharp distinctive pattern only for separation with relatively high reference velocities, as the range of variation of shear stress is higher for higher velocities. Figure 16(a) depicts the surface-streamline pattern on the floor of the test section upstream of the flat plate, with the ceiling contour removed so that there is no streamwise pressure gradient there. In figure 16(b), the corresponding surface flow-visualization in the presence of adverse pressure gradient (imposed by the ceiling contour on the flat plate, with a setting slightly different from that depicted in figure 1) is shown, and this reveals the footprints of the time-averaged extent of the separation bubble; both these visualizations have been done at a speed of $U_{ref} = 9.03\,\mathrm{m\,s^{-1}}$. All the streaks in figure 16(a) point in the downstream direction, parallel to the tunnel centreline (within the experimental uncertainty) indicating that the oncoming flow is nominally two-dimensional and thus establishing the good spanwise uniformity of the test-section flow. The separation and reattachment lines (marked S and R respectively) shown in figure 16(b) can be fairly accurately located using this technique, as the streaks are virtually non-existent due to low values of skin friction close to the mean separation and reattachment lines. The separation and reattachment lines are seen to be approximately straight and normal to the oncoming flow. The streaks downstream of the separation line and upstream of the reattachment line point in the upstream direction due to the presence of reversed flow as expected.

Furthermore, it is clearly seen in figure 16(b) that inside the separation-bubble region, the inverted streaks are not everywhere parallel to the plate centreline and in most of the places have a component in the spanwise direction as well. In order to have a clearer picture of this behaviour close to the separation and reattachment lines, a small portion of the surface-streamline pattern around the plate centreline (having the width of 100 mm) is shown in figure 17(a, b) for $U_{ref} = 9.03\,\mathrm{m\,s^{-1}}$ (corresponding to figure 16b) and $5.4\,\mathrm{m\,s^{-1}}$ respectively. Such a three-dimensional nature of the flow downstream of separation is a well-known feature of many nominally two-dimensional separated flows (see Watmuff 1999). It is, however, interesting to note that the flow upstream of the separation line also shows a certain degree of three-dimensionality even though the oncoming flow is two-dimensional. This intriguing presence of three-dimensionality upstream of the separation line was observed by Watmuff (1999) also in his hot-wire measurements (shown in figure 7a in his paper). The occurrence of

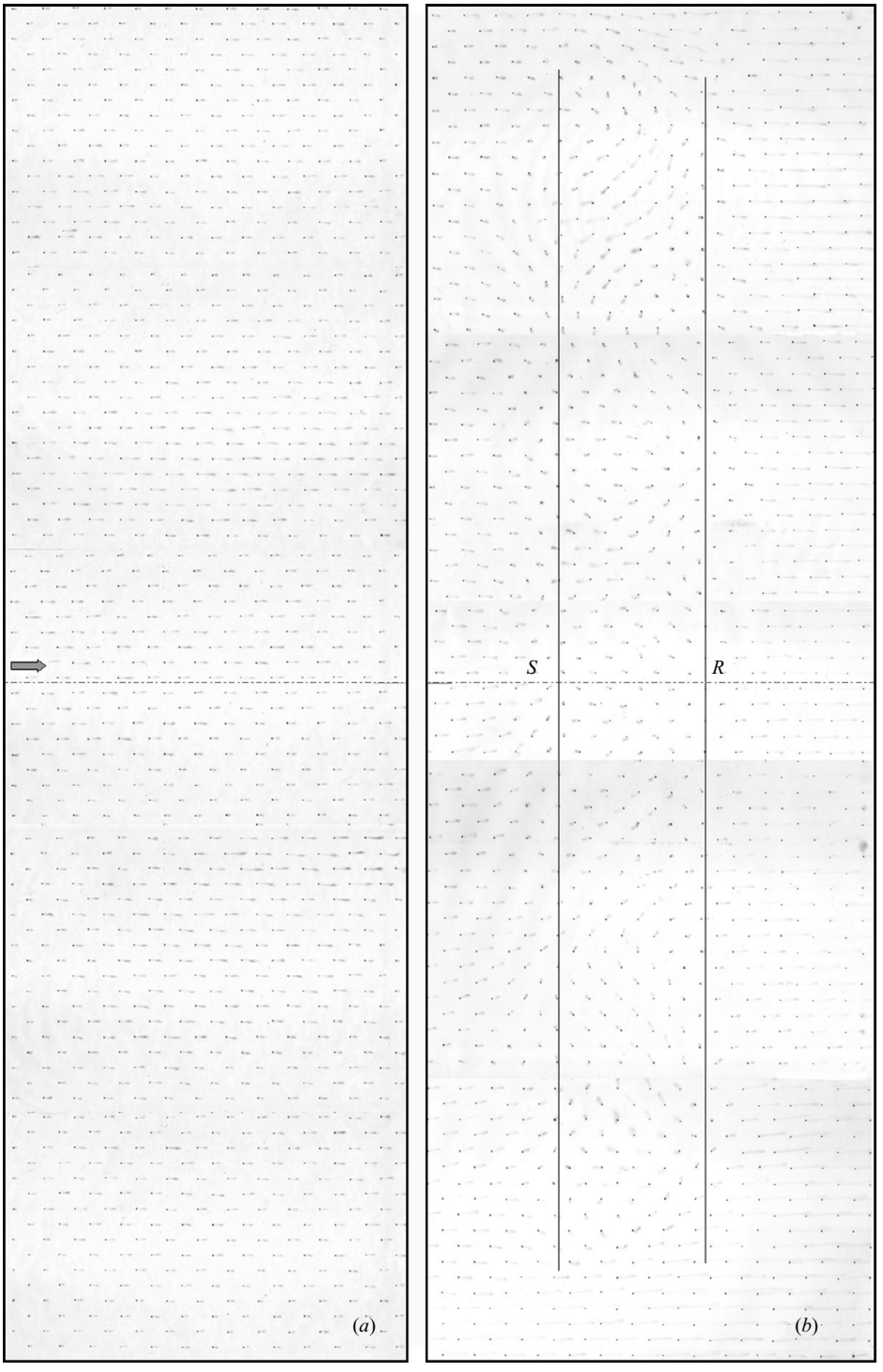

FIGURE 16. (*a*) Ink-dot-matrix flow visualization on the tunnel floor upstream of the plate, with zero pressure gradient imposed in the test section. (*b*) Visualization consisting of separation bubble; $U_{ref} = 9.03\,\mathrm{m\,s^{-1}}$ with separation on the flat plate created by the ceiling contour. Note that the width of the picture is 900 mm, whereas the width of the tunnel is 1000 mm. The flow is from left to right in both the cases.

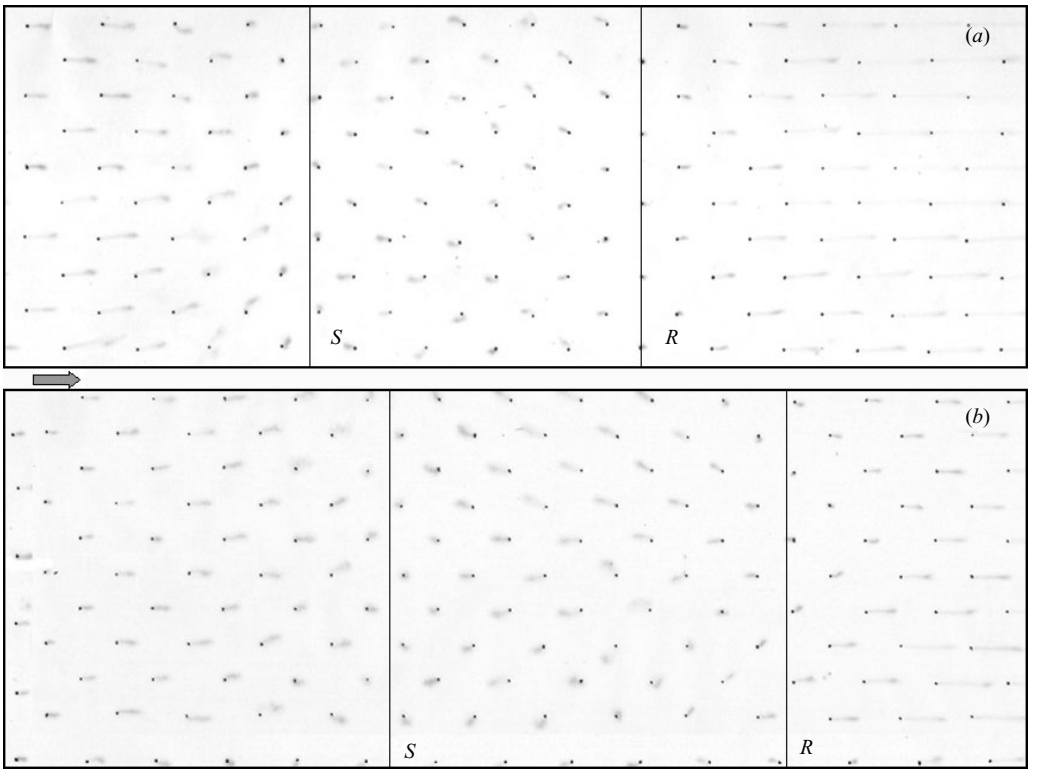

FIGURE 17. A portion of the surface-streamline pattern about the centreline (having the width of 100 mm) for (*a*) $U_{ref} = 9.03\,\mathrm{m\,s^{-1}}$ and (*b*) $U_{ref} = 5.4\,\mathrm{m\,s^{-1}}$.

three-dimensionality close to separation in a nominally two-dimensional oncoming flow has come to be recognized as a topological necessity in recent years in the literature. Theofilis *et al.* (2000) have theoretically shown that a two-dimensional separation line with all the oncoming streamlines normal to it gives rise to an infinite sequence of saddle points. The saddle–saddle connections are 'structurally unstable' and thereby result in a finite number of critical points (at which the streamline slope is indeterminate) on the separation line, which either attract or repel the streamline trajectories. As a result, the streamlines which are straight and parallel to the plate centreline well upstream of separation are bent sideways as the separation line is approached. This gives rise to the observed three-dimensionality upstream of the separation line. The rich topological structure of the surface-streamline patterns, as seen here, is being pursued as a separate investigation.

In order to provide more details of the three-dimensionality of the flow close to the separation line, we have measured surface-pressure distribution for three different spanwise locations (z) for $U_{ref} = 5.4\,\mathrm{m\,s^{-1}}$ (corresponding to figure 17*b*) and is plotted in figure 18. All the three C_p distributions are seen to be in reasonable agreement with each other; the maximum deviation close to the separation location (which is the region of interest here) is found to be 4 %, and that close to the reattachment location is found to be about 9 % of the centreline value. Moreover, the C_p distributions for $z = -125\,\mathrm{mm}$ and $z = 125\,\mathrm{mm}$ show a fairly good collapse onto each other, indicating the presence of a fair degree of symmetry in the pressure distribution about the centreline.

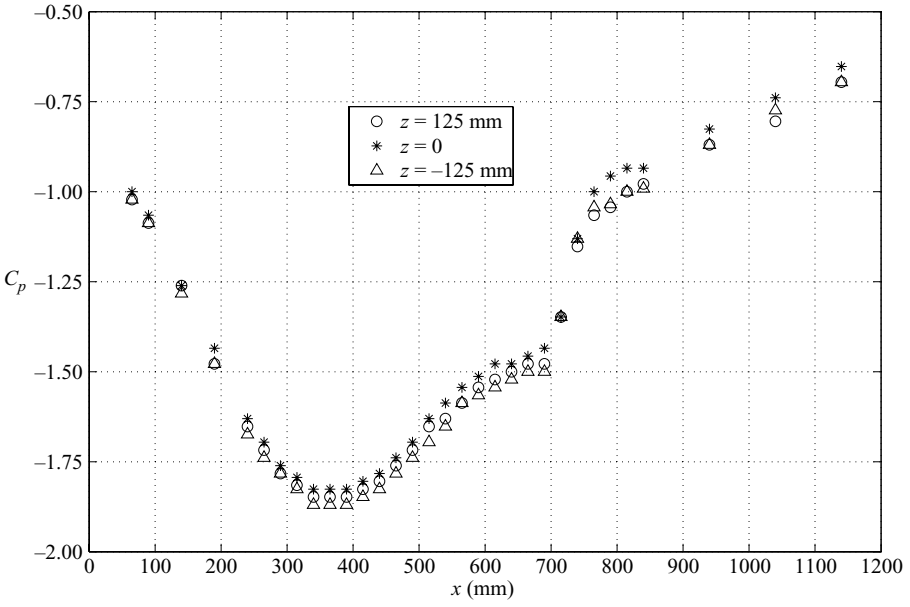

FIGURE 18. Distribution of C_p with x for three different spanwise locations (z); $U_{ref} = 5.4\,\mathrm{m\,s^{-1}}$ (for the conditions corresponding to figure 17*b*).

It was mentioned in § 2 that all the hot-wire measurements had been done along the centreline of the plate. In view of the three-dimensional nature of the flow close to the wall in the vicinity of the separation line (as seen from figures 16*b* and 17), a question may be raised about the utility of centreline measurements and how representative they are of the separation-bubble measurements. A careful look at figure 16(*b*) reveals that the surface-streamline pattern is very nearly symmetric about the centreline. This is also reflected in the pressure distributions shown in figure 18 as already mentioned above. The centreline plane thus corresponds to the symmetry plane of the flow, and it has been a standard practice in the literature to measure the flow field in the symmetry plane of the three-dimensional spanwise symmetric mean flows. For example, Watmuff (1999) has reported extensive measurements along the centre plane, even though he had recognized the surface-flow pattern to have a three-dimensional symmetric structure about the centreline. Furthermore, there are other contexts in fluid dynamics that are replete with symmetric spanwise patterns of three-dimensionality but where measurements are presented on the centreline, e.g. the well-known work of Cantwell, Coles & Dimotakis (1978) in which they have measured the flow in a turbulent spot using laser Doppler velocimetry in the symmetry plane.

Appendix B. Inviscid stability analysis of a piecewise linear profile

In the following, we perform an inviscid spatial stability analysis of a piecewise linear velocity profile adjacent to a solid wall. This is expected to be an approximate representation of what happens in a separation bubble in its essential aspects. Consider the profile shown in figure 19 and given as

$$\begin{aligned} U &= U_1 && \text{for} \quad -L \leqslant y \leqslant 0, \\ U &= U_1 + (U_2 - U1)\frac{y}{\delta_\omega} && \text{for} \quad 0 \leqslant y \leqslant \delta_\omega, \\ U &= U_2 && \text{for} \quad \delta_\omega \leqslant y. \end{aligned} \tag{B 1}$$

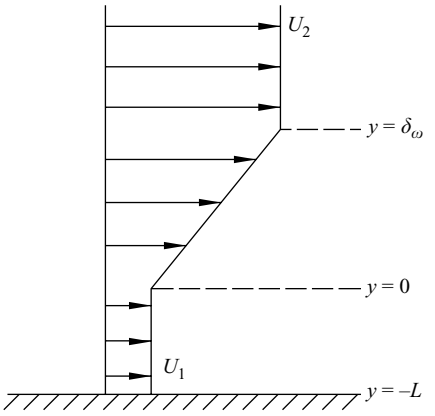

FIGURE 19. Three-piece linear profile in the presence of wall.

We use the Rayleigh equation given by

$$(U - c)(\phi'' - \alpha^2\phi) - U''\phi = 0, \tag{B 2}$$

where $c = \omega/\alpha = c_r + \mathrm{i}\, c_i$ and the symbols carry their usual meaning. The equation has been written in dimensional form.

We apply this equation in the region in which the velocity gradient is continuous and constant, thereby implying $U'' = 0$. This reduces the Rayleigh equation to

$$(U - c)(\phi'' - \alpha^2\phi) = 0. \tag{B 3}$$

For $c_i \neq 0$ (growing modes), $(U - c) \neq 0$. This gives

$$(\phi'' - \alpha^2\phi) = 0, \tag{B 4}$$

for which the solutions can be written at once as

$$\phi = P\mathrm{e}^{(\alpha y)} + Q\mathrm{e}^{(-\alpha y)}. \tag{B 5}$$

The boundary conditions are

$$y \to \infty;\ \phi \to 0, \quad \text{and} \quad y = -L;\ \phi = 0. \tag{B 6}$$

Applying these boundary conditions we get

$$\begin{aligned} \phi &= Q_1\left(\mathrm{e}^{(-\alpha y)} - \mathrm{e}^{(2\alpha L)}\mathrm{e}^{(\alpha y)}\right) && \text{for} \quad -L \leqslant y \leqslant 0, \\ \phi &= P_2\mathrm{e}^{(\alpha y)} + Q_2\mathrm{e}^{(-\alpha y)} && \text{for} \quad 0 \leqslant y \leqslant \delta_\omega, \\ \phi &= Q_3\mathrm{e}^{(-\alpha y)} && \text{for} \quad \delta_\omega \leqslant y, \end{aligned} \tag{B 7}$$

where Q_1, Q_2, Q_3 and P_2 are arbitrary constants.

Two matching conditions need to be satisfied at each corner (i.e. $y = 0$ and $y = \delta_\omega$). These are (Drazin & Reid 1981):

(a) continuity of particle displacement, $[\phi/(U - c)]_{y^-} = [\phi/(U - c)]_{y^+}$;

(b) continuity of pressure, $[(U - c)(\mathrm{d}\phi/\mathrm{d}y) - \phi(\mathrm{d}U/\mathrm{d}y)]_{y^-} = [(U - c)(\mathrm{d}\phi/\mathrm{d}y) - \phi(\mathrm{d}U/\mathrm{d}y)]_{y^+}$; where the quantity in the square bracket is the fluctuating pressure amplitude.

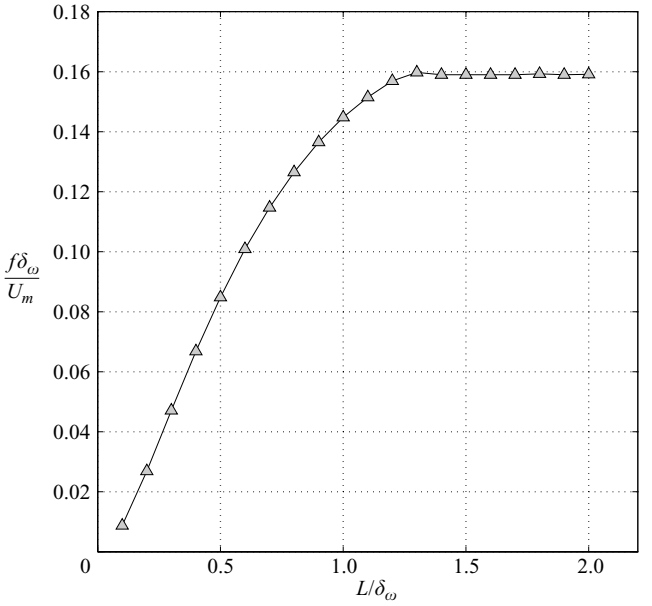

FIGURE 20. Variation of the most amplified frequency with L/δ_ω, for the piecewise linear profile with $\lambda = 1$.

Employing these conditions and eliminating the arbitrary constants, we obtain the dispersion relation which can be written in a non-dimensional form as

$$\frac{\left[\lambda - \overline{\alpha}\dfrac{(1-\lambda-\overline{c})}{(1-\mathrm{e}^{2\overline{\alpha}L/\delta_\omega})}\right]}{\mathrm{e}^{\overline{\alpha}}[\overline{\alpha}(1+\lambda-\overline{c})-\lambda]} = \frac{\left[\overline{\alpha}\dfrac{(1-\lambda-\overline{c})\mathrm{e}^{2\overline{\alpha}L/\delta_\omega}}{(1-\mathrm{e}^{2\overline{\alpha}L/\delta_\omega})} - \lambda\right]}{\lambda \mathrm{e}^{-\overline{\alpha}}}, \tag{B 8}$$

where $\overline{\alpha} = \alpha\delta_\omega$; $\overline{c} = c/U_m$; $U_m = (U_1 + U_2)/2$; and $\lambda = (U_2 - U_1)/U_2 + U_1$. The profile we choose is the one with $\lambda = 1$ (i.e. $U_1 = 0$) which is similar to the separation velocity profile. It also approximates the profiles in the initial portion of the dead-air region downstream of separation, where the backflow is very weak.

We have numerically solved the above dispersion relation for the spatial stability problem. The result of that is shown in the figure 20 in which the most amplified frequency is plotted as a function of the non-dimensional distance from the wall (L/δ_ω).

In the following, we modify the frequency scaling arising from inviscid theory in the presence of wall, by using heuristic physical arguments, and thereby construct the most appropriate non-dimensional form for the most amplified frequency. Towards this, we are guided by the work of Villermaux (1998). He performed temporal stability analysis of a mixing layer wherein the effect of viscous correction to the most amplified wavenumber was the focus. However, the viscous correction in his study was not so much due to wall proximity (which is of relevance to the present context) as due to the viscous spreading of the vortex sheet with time. In the course of his analysis, Villermaux (1998) arrived at a mean square length scale $-(\delta_\omega/2)^2 + 2a(\sqrt{\nu t})^2$, where '$a$' is a shape parameter and δ_ω is the initial vorticity thickness, based on viscous-diffusion considerations. The essential physics of Villermaux's work (Villermaux 1998) is that there is a destabilizing influence due to the shear (which is idealized by a vortex sheet of certain initial thickness), which would lead to the growth of disturbances

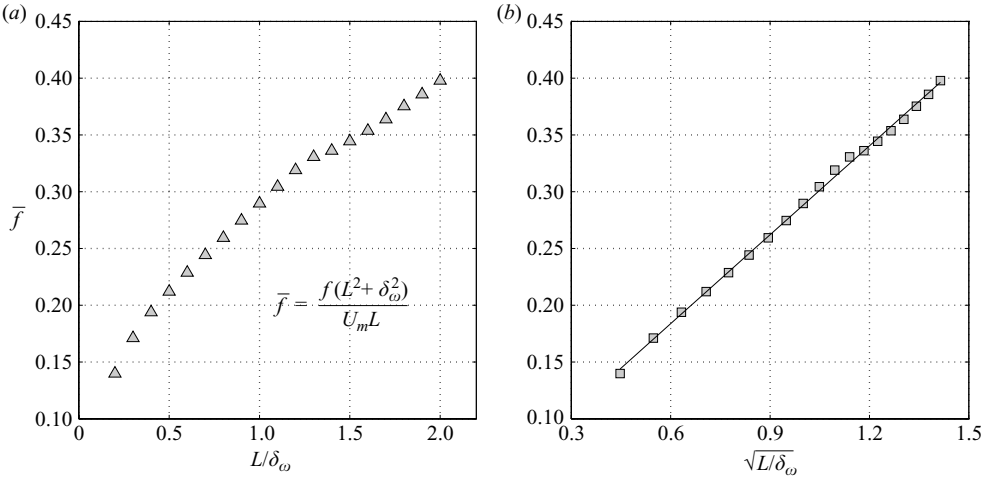

FIGURE 21. Variation of the most amplified frequency in a rescaled form with (*a*) L/δ_ω and (*b*) $\sqrt{L/\delta_\omega}$, for $\lambda = 1$.

competing against the stabilizing influence due to the viscous diffusion of the vortex sheet (which will weaken the shear). By consideration along these lines, he was able to arrive at a viscous correction to the mixing-layer problem.

In the present problem, the diffusion of a vortex sheet of initial thickness δ_ω that is located at a distance L from the wall is considered. A mean square length can be constructed as $\delta_\omega^2 + L^2$, with the recognition that the stabilizing effect of viscous diffusion is likely to be active till the diffused vortex sheet reaches the wall. The control parameter or the independent variable is taken to be the non-dimensional distance from the wall L/δ_ω. The most amplified frequency in the problem is scaled as $f(\delta_\omega^2 + L^2)/\nu$. This quantity can be expected to be a function of the Reynolds number $U_m L/\nu$ for a given value of L/δ_ω, from the functional relationship $f = F(U_m, L, \nu, \delta_\omega)$ similar to that given in § 5. We can construct a new non-dimensional form for the most amplified frequency by taking ratio of the non-dimensional parameters $f(\delta_\omega^2 + L^2)/\nu$ and $U_m L/\nu$, and this is given by $f(\delta_\omega^2 + L^2)/(U_m L)$. This can be rewritten as $f(L + \delta_\omega^2/L)/U_m$ and can be interpreted roughly as a ratio of time scales – that of the mean velocity gradient to that of the most amplified wave given by inviscid instability. For a consistency check, let us examine this term in the limit $L \to 0$ (with non-zero δ_ω); i.e. the vortex sheet moving towards the wall. The non-dimensional frequency becomes $f\delta_\omega^2/(U_m L)$. In order that there is no singularity as $L \to 0$, we would require $f \to 0$ corresponding to $f(L + \delta_\omega^2/L)/U_m \to 0$ as the wall is reached (i.e. $L/\delta_\omega \to 0$). This is of course physically consistent – as the vortex sheet moves to the wall, there is complete stabilizing influence on the vortex sheet due to the restraining (inviscid) boundary conditions at the wall, and this results in the limit $f \to 0$, as seen in figure 20. (It also follows from a similar analysis that when $L = 0$, the profile is inviscidly stable.) It should be noted that if fL/U_m were to be used as the parameter based on a simple-minded thinking (rather than the form $f(L + \delta_\omega^2/L)/U_m$ introduced here), it will not retrieve the result $f \to 0$ as $L \to 0$ as seen in figure 20 (as then f can still be non-zero with vortex sheet at the wall, a physically inconsistent result). In view of this, the correction term δ_ω^2/L is required in the definition of the length scale.

A plot of $f(L + \delta_\omega^2/L)/U_m$ versus L/δ_ω can now be easily constructed, and this is seen to be approximately of the form of a parabola as can be seen in figure 21(*a*).

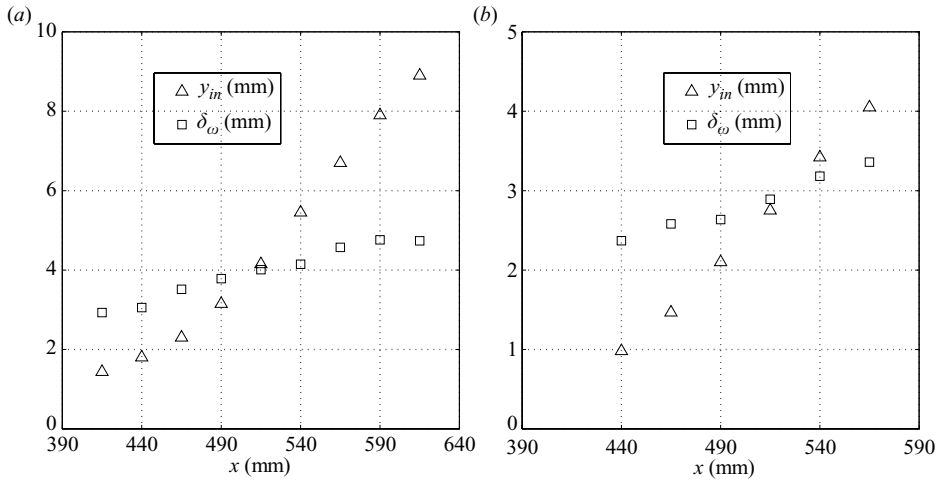

FIGURE 22. Variation of the distance of inflection point y_{in} and the vorticity thickness δ_ω with the streamwise coordinate x, for (*a*) $U_{ref} = 2.78\,\mathrm{m\,s^{-1}}$ and (*b*) $U_{ref} = 5.4\,\mathrm{m\,s^{-1}}$.

Instead $f(L+\delta_\omega^2/L)/U_m$ is plotted against $\sqrt{L/\delta_\omega}$ resulting in an almost linear variation as is evident from figure 21(*b*).

Hence if we take $f(L+\delta_\omega^2/L)/U_m = f(L^2+\delta_\omega^2)/(U_m L) \sim \sqrt{L/\delta_\omega}$ based on the result in figure 21(*b*), we can rearrange this as $f(L^2+\delta_\omega^2)/\nu \sim (U_m L/\nu)\sqrt{L/\delta_\omega}$. This result for a piecewise linear profile, obtained from an inviscid instability analysis and modified for wall-proximity effects by heuristic physical considerations, can be applied to the separation-bubble problem by replacing L by y_{in} and U_m by U_{in}. This results in $f(y_{in}^2+\delta_\omega^2)/\nu \sim (U_{in}\,y_{in}/\nu)\sqrt{y_{in}/\delta_\omega}$. As discussed in § 5, this scaling principle for the most amplified frequency is found to be in excellent agreement with the results of the Rayleigh and Orr–Sommerfeld calculations for the actual profiles close to the separation point.

Appendix C. Variation of dimensional quantities in streamwise direction

In order to further clarify the rationale behind choosing the relevant scaling parameters and their appropriate combination to form the non-dimensional groups, we consider variation of dimensional quantities such as y_{in}, δ_ω and f with the streamwise distance, x in this appendix.

Figure 22(*a*, *b*) shows the variation of y_{in} and δ_ω for two different reference speeds, $U_{ref} = 2.78\,\mathrm{m\,s^{-1}}$ and $U_{ref} = 5.4\,\mathrm{m\,s^{-1}}$ respectively (for the ceiling setting shown in figure 1).

The reasons for choosing y_{in} and δ_ω as the relevant length scales for non-dimensionalizing the frequency have already been made clear in the main text. The separation-bubble problem consists of features of both wall-bounded and free shear layers. Since the dominant instability mechanism is inflectional in character, the vorticity thickness associated with the inflection point arises as a natural length scale. However, since the tempering effect of the wall cannot be neglected for a separated shear layer, the distance of the inflection point from the wall serves as another important length scale in the problem. Both the length scales, y_{in} and δ_ω, are thus necessary to adequately characterize the instability dynamics of separation

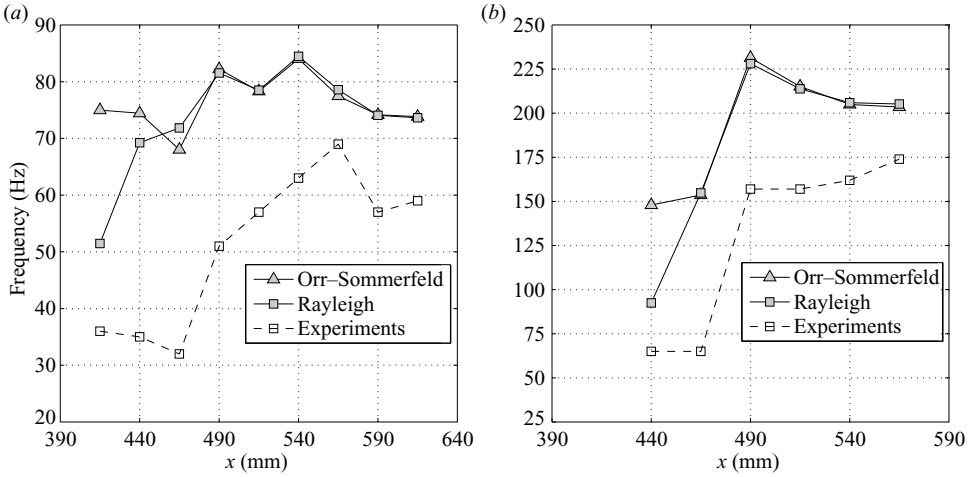

FIGURE 23. Variation of the dimensional frequency with the streamwise coordinate x, for (a) $U_{ref} = 2.78\,\mathrm{m\,s^{-1}}$ and (b) $U_{ref} = 5.4\,\mathrm{m\,s^{-1}}$.

bubbles. Figure 22(a,b) shows that the curves of y_{in} and δ_ω cross each other somewhere downstream of separation; upstream of the crossover point, y_{in} is less than δ_ω, whereas the relation becomes opposite after the crossover takes place. This behaviour suggests that y_{in} or δ_ω alone is not sufficient, and therefore some combination of these two length scales must be sought for scaling the frequency.

The distribution of dimensional frequency (in Hz) with x is plotted in figure 23(a,b). The figure includes most amplified frequencies obtained from the Orr–Sommerfeld and Rayleigh analyses and the dominant frequencies observed in the measurements. It is evident that the frequencies are not constant in the downstream direction and vary in a nonlinear fashion. The frequencies are expected to be different for different streamwise stations, as the base velocity profiles which dictate the local linear instability dynamics are different. The striking linear behaviour observed in figure 10 in the main text, in the region of interest, is thus as a result of the mean square combination of y_{in} and δ_ω as has been explained in Appendix B.

REFERENCES

ALAM, M. & SANDHAM, N. D. 2000 Direct numerical simulation of 'short' laminar separation bubbles with turbulent reattachment. *J. Fluid Mech.* **410**, 1–28.

BENDAT, J. S. & PIERSOL, A. G. 1966 *Measurement and Analysis of Random Data*. John Wiley & Sons.

BETCHOV, R. & CRIMINALE, W. O. 1967 *Stability of Parallel Flows*. Academic.

BETCHOV, R. & SZEWCZYK, A. 1963 Stability of a shear layer between parallel streams. *Phys. Fluids* **6** (10), 1391–1396.

BOIKO, A. V., GREK, G. R., DOVGAL, A. V. & KOZLOV, V. V. 2002 *The Origin of Turbulence in Near-Wall Flows*. Springer.

CANTWELL, B. J., COLES, D. & DIMOTAKIS, P. E. 1978 Structure and entrainment in the plane of symmetry of a turbulent spot. *J. Fluid Mech.* **87**, 641–672.

DAS, D. 1998 Evolution and instability of unsteady boundary-layers with reverse flow. PhD thesis, Department of Mechanical Engineering, Indian Institute of Science, Bangalore, India.

DOVGAL, A. V., KOZLOV, V. V. & MICHALKE, A. 1994 Laminar boundary layer separation: instability and associated phenomena. *Prog. Aerosp. Sci.* **30**, 61–94.

Drazin, P. G. & Reid, W. H. 1981 *Hydrodynamic Stability*. Cambridge University Press.

Eaton, J .K. & Johnston, J. P. 1980 Turbulent flow reattachment: an experimental study of the flow and structure behind a backward-facing step. *Tech Rep.* MD-39. Deparment of Mechanical Engineering, Stanford University.

Fitzgerald, E. J. & Mueller, T. J. 1990 Measurements in a separation bubble on an airfoil using laser velocimetry. *AIAA J.* **28** (4), 584–592.

Gaster, M. 1967 The structure and behaviour of separation bubbles. *ARC London R&M* (3595).

Gaster, M. & Grant, I. 1975 An experimental investigation of the formation and development of a wave packet in a laminar boundary layer. *Proc. R. Soc. Lond.* A **347**, 253–269.

Haggmark, C. P., Bakchinov, A. A. & Alfredsson, P. H. 2000 Experiments on a two-dimensional laminar separation bubble. *Phil. Trans. R. Soc. Lond.* A **358**, 3193–3205.

Hammond, D. A. & Redekopp, L. G. 1998 Local and global instability properties of separation bubbles. *Eur. J. Mech.* B **17** (2), 145–164.

Hatman, A. & Wang, T. 1998 Separated-flow transition. Part 1. Experimental methodology and mode classification. *Paper* 98-GT-461. ASME.

Healey, J. J. 1998 Characterizing boundary-layer instability at finite Reynolds numbers. *Eur. J. Mech.* B **17** (2), 219–237.

Herbert, T. 1988 Secondary instability of boundary layers. *Annu. Rev. Fluid Mech.* **20**, 487–526.

Horton, H. P. 1969 A semi-empirical theory for the growth and bursting of laminar separation bubbles. *ARC London* (C.P. No. 1073).

Lang, M., Rist, U. & Wagner, S. 2004 Investigations on controlled transition development in a laminar separation bubble by means of LDA and PIV. *Exp. Fluids* **36**, 43–52.

Langston, L. S. & Boyle, M. T. 1982 A new surface-streamline flow-visualisation technique. *J. Fluid Mech.* **125**, 53–57.

Marxen, O., Lang, M., Rist, U. & Wagner, S. 2003 A combined experimental/ numerical study of unsteady phenomena in a laminar separation bubble. *Flow Turbul. Combust.* **71**, 133–146.

Maslowe, S. A. 1986 Critical layers in shear flows. *Annu. Rev. Fluid Mech.* **18**, 405–432.

Maucher, U., Rist, U. & Wagner, S. 1999 Transitional structures in a laminar separation bubble. In *New Results in Numerical and Experimental Fluid Mechanics II* (ed. W. Nitsche, H. J. Heinemann & R. Hilbig), vol. 72, pp. 307–314. Vieweg.

Michalke, A. 1964 On the inviscid instability of the hyperbolic-tangent velocity profile. *J. Fluid Mech.* **19**, 543–556.

Monkewitz, P. A. & Huerre, P. 1982 Influence of the velocity ratio on the spatial instability of mixing layers. *Phys. Fluids* **25** (7), 1137–1143.

Narasimha, R. & Prasad, S. N. 1994 Leading edge shape for flat plate boundary layer studies. *Exp. Fluids* **17** (5), 358–360.

Nayfeh, A. H., Ragab, S. A. & Masad, J. A. 1990 Effect of a bulge on the subharmonic instability of boundary layers. *Phys. Fluids* A **2** (6), 937–948.

Niew, T. R. 1993 The stability of the flow in a laminar separation bubble. PhD thesis, St John's College, Cambridge.

Pauley, L. L., Moin, P. & Reynolds, W. C. 1990 The structure of two-dimensional separation. *J. Fluid Mech.* **220**, 397–411.

Ramesh, O. N., Hodson, H. P. & Harvey, N. W. 2001 Separation control in ultra-high lift aerofoils by unsteadiness and surface roughness. In *Proc. of the Intl Society of Airbreathing Engines ISABE-1096*, Bangalore, India.

Rist, U., Maucher, U. & Wagner, S. 1996 Direct numerical simulation of some fundamental problems related to transition in laminar separation bubbles. In *Computational Fluid Dynamics '96* (ed. J. A. Desideri, C. Hirsch, P. Le Tallec, M. Pandolfi & J. Periaux), pp. 319–325. John Wiley & Sons.

Schlichting, H. 1960 *Boundary Layer Theory*. McGraw-Hill.

Sinha, S. N., Gupta, A. K. & Oberai, M. M. 1981 Laminar separating flow over backsteps and cavities. Part 1. Backsteps. *AIAA J.* **19**, 1527–1530.

Spalart, P. R. & Strelets, M. Kh. 2000 Mechanisms of transition and heat transfer in a separation bubble. *J. Fluid Mech.* **403**, 329–349.

Taghavi, H. & Wazzan, A. R. 1974 Spatial stability of some Falkner–Skan profiles with reversed flow. *Phys. Fluids* **17** (12), 2181–2183.

Tani, I. 1964 Low speed flows involving bubble separations. *Prog. Aerosp. Sci.* **5**, 70–103.

Theofilis, V., Hein, S. & Dallmann, U. 2000 On the origins of unsteadiness and three-dimensionality in a laminar separation bubble. *Phil. Trans. R. Soc. Lond.* A **358**, 3229–3246.

VanDyke, M. 1982 *An Album of Fluid Motion*. Parabolic.

Villermaux, E. 1998 On the role of viscosity in shear instabilities. *Phys. Fluids* **10** (2), 368–373.

Watmuff, J. H. 1999 Evolution of a wave packet into vortex loops in a laminar separation bubble. *J. Fluid Mech.* **397**, 119–169.

Zaman, K. B. M. Q. & Hussain, A. K. M. F. 1981 Turbulence suppression in free shear flows by controlled excitation. *J. Fluid Mech.* **103**, 133–159.